*Annu. Rev. Biophys. Biomol. Struct. 1999. 28:319–65*


# MEMBRANE PROTEIN FOLDING AND STABILITY: Physical Principles

*Stephen H. White*
Department of Physiology and Biophysics, University of California at Irvine, Irvine, California 92697-4560; e-mail: blanco@helium.biomol.uci.edu

*William C. Wimley*
Department of Biochemistry, Tulane University Medical Center, New Orleans, Louisiana 70112-2739; e-mail: wwimley@mailhost.tcs.tulane.edu

KEY WORDS: lipid-protein interactions, peptide-bilayer interactions, membrane-active peptides, antimicrobial peptides, thermodynamics, bilayer structure, soluble protein folding

ABSTRACT

Stably folded membrane proteins reside in a free energy minimum determined by the interactions of the peptide chains with each other, the lipid bilayer hydrocarbon core, the bilayer interface, and with water. The prediction of three-dimensional structure from sequence requires a detailed understanding of these interactions. Progress toward this objective is summarized in this review by means of a thermodynamic framework for describing membrane protein folding and stability. The framework includes a coherent thermodynamic formalism for determining and describing the energetics of peptide-bilayer interactions and a review of the properties of the environment of membrane proteins—the bilayer milieu. Using a four-step thermodynamic cycle as a guide, advances in three main aspects of membrane protein folding energetics are discussed: protein binding and folding in bilayer interfaces, transmembrane helix insertion, and helix-helix interactions. The concepts of membrane protein stability that emerge provide insights to fundamental issues of protein folding.

CONTENTS





1056-8700/99/0610-0319$08.00

# PERSPECTIVES AND OVERVIEW

## *Introduction*

Only two structural motifs (Figure 1) have been observed for membrane proteins (MPs): membrane-spanning $\alpha$-helix bundles and $\beta$-barrels, the former being predominant. Analyses of the complete genomic sequences for several organisms indicate that 20–30% of all open reading frames code for the helix-bundle motif (4, 157). A frequently observed submotif is interfacial helices connected to adjacent transmembrane (TM) helices, illustrated by the fd coat protein. As shown schematically in Figure 1, the secondary structure elements of MPs are in contact with each other, the bilayer HC core, the bilayer interface, and, of course, water. The prediction of MP structure and stability requires that the energetics of the interactions of the peptide chains with each other and with the various components of their environment be understood.

We present a comprehensive summary of our current understanding of these energetics using a coherent thermodynamic approach that may help set some directions for further progress. The presentation is organized around several guiding questions: What are the general features of MPs? How are they assembled? How can their thermodynamic stability be described? What is the nature of the lipid bilayer as a host phase for MPs? What are the dominant forces that determine structure and stability? What can the folding and stability of MPs tell us about the protein folding problem generally?

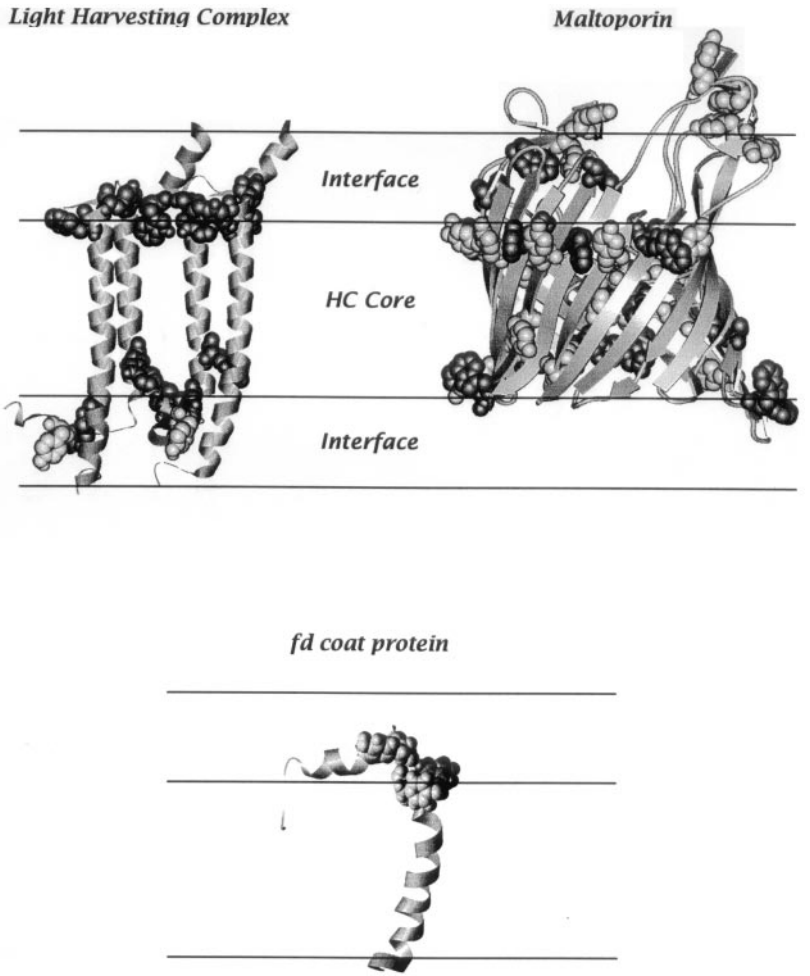


*Figure 1* Examples of the two known structural motifs of membrane proteins, the $\alpha$-helix bundle and the $\beta$-barrel. The bundle motif is illustrated by a few subunits of the light harvesting complex II of *Rhodospirillum molischianum* (74) (PDB coördinates 1LGH) and the $\beta$-barrel motif by maltoporin of *Salmonella typhimurium* (97) (PDB coördinates 2MPR), both determined by X-ray crystallography. The membrane is comprised of interfacial regions, each about 15 Å thick, and the hydrocarbon (HC) core, which has a thickness of about 30 Å (see Figure 6). Various parts of the proteins interact with both of these regions. The average length of the helices in three $\alpha$-helix bundle proteins is $38 \pm 7$ Å ($25 \pm 5$AA) [computed from data in (17)]. A submotif of the helix-bundle is interfacial helices lying parallel to the membrane plane as illustrated in the lower panel by the coat protein of fd bacteriophage whose structure has been determined by NMR methods (96) (PDB coordinates 1FDM). The $C_\alpha$ backbones are shown as ribbons. The tryptophan and tyrosine side chains, located characteristically at the membrane surfaces for all known membrane proteins, are shown as black and gray space-filling models, respectively.

## *Structural Features of Membrane Proteins*

The general structural and thermodynamic characteristics of soluble proteins had been well established and amply reviewed (24, 69, 123, 126, 129) by the time the first high-resolution crystallographic structure of an MP had been determined (31). The crystallographic structures of a dozen or so MPs are now known to high resolution (Table 1; two examples are shown in Figure 1). How do their general structural features compare with those of soluble proteins? The answer is: remarkably well (17, 27, 80, 118, 120, 183). A close examination (120, 183) of one of the early crystallographic structures, the photosynthetic reaction center (PSRC) of *Rhodobacter sphaeroides*, revealed that the interior amino acids were almost exclusively nonpolar and packed just as tightly as those of soluble proteins, as suggested earlier by measurements of the partial specific volume of bacteriorhodopsin (150). Except for coordination between four histidines on TM helices with the heme iron, H-bonds between secondary structure elements in PSRC were rare and salt-bridges nonexistent. These observations have generally held true for subsequent structures (17, 27, 80, 156), except for pore-forming proteins such as the porins (Figure 1), whose deepest interiors are water-filled [but so are those of some soluble proteins, such as tryptophan synthase (56)]. Salt-bridges exist and are functionally important in

**Table 1** Integral membrane proteins whose crystallographic structures have been determined to 4 Å or better resolution [based upon and revised from Preusch et al (115)][a]

| Protein | Protein Data Bank codes (References) |
|---|---|
| Bacteriorhodopsin | 2BRD (44, 48), 1AT9 (71), 1AP9 (109), 1BRX (87) |
| Bacterial photosynthetic reaction centers | 1PRC (33), 1PSS (183), 2RCR (21) |
| Light-harvesting complexes | 1KZU (95), 1LGH (74) |
| Photosystem I | 2PPS (135) |
| Porins (multimeric) | 2POR (159, 160), 1OPF (26), 1PHO (26), 2MPR (97) |
| Porins (monomeric) | 1BXW (108a), 1FCP (42a), 2FCP (42a) 1FEP (19a) |
| $\alpha$-hemolysin | 7AHL (143) |
| Prostaglandin synthases | 1PRH (111), 1CX2 (75) |
| Cytochrome oxidases | 1OCC (151), 1AR1 (58) |
| Cytochrome $bc_1$ complex | 1QCR (180), 1BCC (188), 1BGY (57) |
| Potassium channel | 1BL8 (36) |
| Mechanosensitive channel | 1MSL (21a) |

[a]Reference is made to all of the protein types whose structures have been determined, but only representative examples and key references are included in this listing. This list is complete as of 1 January 1999. A current list, with links to the Protein Data Bank, is maintained at the Stephen White Laboratory worldwide web site (http://blanco.biomol.uci.edu).

some transport proteins (65, 76), but direct measurements of salt-bridge solvation energies of model peptides in octanol/water systems (175) and studies of soluble proteins (49, 155) suggest that they are energetically neutral in terms of stability. The interiors of MPs are thus similar to those of soluble proteins. The early hypothesis that MPs might be "inside-out proteins" stabilized mostly by polar interactions does not appear to be correct.

Also in the manner of soluble proteins, the interiors of MPs are comprised of internally H-bonded $\alpha$-helices and $\beta$-sheets. Major portions of their masses are buried within the HC core of the membrane and arranged so that their outer surfaces face the HC core. Although the average hydrophobicity of the interiors of MPs are the same as for soluble proteins, the amino acids of these outer surfaces are more hydrophobic (119, 132). The average lengths of the traversing secondary structure elements are greater than for soluble proteins so that the 30 Å thick bilayer HC core can be spanned: $\alpha$-helices are generally longer than 20 amino acids (1.5 Å/residue), and $\beta$-strands longer than 10 amino acids (3.3 Å/residue). Because of the length and the highly nonpolar character of TM helices, hydropathy plots (39, 77, 128, 163) have proven to be extraordinarily useful and remarkably accurate for predicting the topology of $\alpha$-helical MPs. Although determination of topology is an important first step toward structure determination, much more could be done with the hydropathy plot approach if the physical principles of MP stability were better understood.

Another distinguishing characteristic of MPs is that they have a direction in space, defined by the membrane normal. Some amino acids have preferred locations along this TM axis. For example, arginine and lysine are much more abundant in the cytoplasmic domains relative to the periplasmic domains of bacterial MPs. This so-called positive-inside rule significantly improved MP topology prediction (153). A dramatic example of a nonuniform TM amino acid distribution is the very high preference of aromatic amino acids, especially tryptophan and tyrosine, for interfacial locations (134). This preference has been observed in all MPs of known three-dimensional structure (Figure 1), and statistical studies of sequence databases indicate that the preference is shared by virtually all MPs (79, 121, 154, 156). A physical basis for the preference and the role it may play in MP folding and stability is addressed below. Wallin et al (156) present an informative analysis of other amino acid preferences in $\alpha$-helix bundle proteins.

## *Assembly of Membrane Proteins and Thermodynamic Equilibrium*

Constitutive MPs are assembled via a complex translocation/insertion process discovered by Blobel & Dobberstein (13), outlined in the top panel of Figure 2. This remarkable process has been summarized in several recent

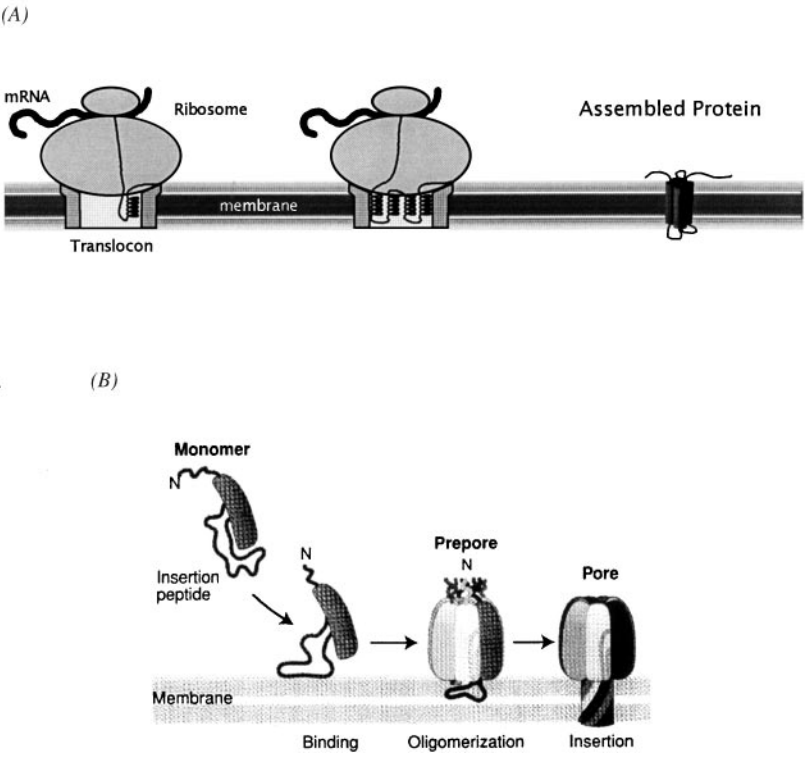


*Figure 2* Mechanisms of membrane protein assembly. (*A*) The *upper frame* shows schematically that constitutive membrane proteins are assembled by a translocation apparatus involving the transient attachment of an active ribosome to a so-called translocon embedded in the membrane. After the protein is synthesized into the translocon and transferred into the membrane, the apparatus disassembles, leaving the protein stably folded in the membrane. The figure is based on the work of several authors (13, 64, 141). (*B*) The *lower frame* shows the assembly of the nonconstitutive membrane protein $\alpha$-hemolysin into a heptameric pore from protomers that are soluble in the aqueous phase, but partition spontaneously into the membrane. The thermodynamic driving force for the assembly is likely to be the favorable thermodynamics of $\beta$-sheet formation on membranes (176). The crystallographic structure of the protein was determined by Song et al (143). Regardless of how a stably folded protein enters the membrane, it resides in a free energy minimum. Its structure and stability are thus determined by the energetics of the interactions of the peptide chains with each other, with the lipid bilayer hydrocarbon core and interface, and with water (see Figure 1). [The figure in the lower frame is reprinted with permission from Engelman (1996) *Science* 274:1850–51. Copyright 1996, American Association for the Advancement of Science.]

reviews (2, 11, 64, 94, 133, 141). In brief, the ribosome secretes nascent chains into membrane-resident translocons, where they are assembled and released into the membrane by a process that is only vaguely understood. After completion of the process, the ribosome-translocon complex dissociates, leaving the protein stably folded in the membrane. Nonconstitutive MPs, such as melittin (32), colicins (28), and diphtheria toxin (184), bypass this elaborate machinery by spontaneously entering the membrane from the aqueous phase. They do this by existing as soluble forms in the aqueous phase and thence bind to membranes where they insert following refolding and/or assembly. A particularly interesting example is the heptameric $\beta$-barrel protein staphylococcal $\alpha$-hemolysin (143) (lower panel of Figure 2).

The large amount of thermodynamic, structural, and functional data available for soluble proteins indicate that they reside structurally in a free energy minimum under normal physiological conditions (35, 124), as first proposed by Anfinsen (3). Membrane proteins would be expected a priori to behave similarly. Indeed, all available evidence suggests that constitutive MPs in situ are in fact equilibrium structures (reviewed in 82). If the final stages of the folding of constitutive MPs are guided by equilibrium thermodynamics, one would expect coexpressed contiguous fragments of MPs to assemble in situ into functional proteins (114). This has been observed to be the case for lactose permease (12), rhodopsin (127), the red cell anion exchanger protein (45), and, remarkably, the $\beta$-barrel MP OmpA (73). Although some toxins and antimicrobial peptides (51) have a transient existence in a TM state, many of them, such as the $\alpha$-hemolysin heptamer (Figure 2), colicins bound to model membranes (reviewed in 28), and the T (transmembrane) domain of diphtheria toxin, can form stable equilibrium structures in lipid vesicles (184).

Regardless of the insertion/assembly process, stably folded MPs reside in a free energy minimum determined by the net energetics of the interactions of the peptide chains with water, each other, the lipid bilayer (hydrocarbon core and interface), and cofactors. The problem of predicting the structure and stability of MPs from sequence is therefore fundamentally a problem of physical chemistry, albeit a difficult one.

## THERMODYNAMICS OF MEMBRANE PROTEINS

### *The Importance of Hydrogen Bonding*

Knowledge of the forces stabilizing soluble proteins has come principally from thermodynamic studies of the folding/unfolding process (124) induced by heat (116) or denaturants (108). This approach has not been used so widely for MPs. The main difficulty, as summarized in a review by Haltia & Freire (46), is that MPs resist complete denaturation, i.e. desorption and/or unfolding of

secondary structure elements, because of the great stability of these elements in membranes. Denaturation arises primarily from the dissociation of multimers, subunits, and secondary structure elements and from the unfolding of extramembrane domains. It is frequently irreversible. Despite these general difficulties, progress has been made using heat (70), denaturants (72, 81, 145), and other methods (15). We discuss below studies of the thermal stability of bacteriorhodopsin (bR) (19, 50, 59, 67).

Figure 3 explains why the secondary structure elements of MPs resist unfolding and/or desorption. The transfer free energy $\Delta G_{CONH}$ of a non-H-bonded peptide bond from water to carbon tetrachloride is about $+6$ kcal mol$^{-1}$, compared with only $+0.6$ kcal mol$^{-1}$ for the transfer free energy $\Delta G_{Hbond}$ of H-bonded peptide bonds (130). Computational studies (7, 10) of the transfer of $\alpha$-helices into an alkane phase suggest values of 6.4 and 2.1 kcal mol$^{-1}$ for $\Delta G_{CONH}$ and $\Delta G_{Hbond}$, respectively. Thus, the per-residue free energy cost of disrupting H-bonds in a membrane, $\Delta G_{CONH} - \Delta G_{Hbond}$, appears to be 4–5 kcal mol$^{-1}$. For a 20 AA TM helix, the total free energy cost would be 80–100 kcal mol$^{-1}$, consistent with the resistance of TM helices to thermal denaturation.

The data of Figure 3 disclose another important issue. The favorable free energy of partitioning the most hydrophobic side chain, tryptophan, into a nonpolar phase cannot overcome $\Delta G_{CONH}$. Whole amino acid residues can enter the HC core only if their peptide bonds are H-bonded. As discussed in detail elsewhere (163, 168), the value of $\Delta G_{Hbond}$ will determine whether or not a largely nonpolar TM helix will be stable across the membrane. Consider, for example, polyalanine and polyleucine helices. If $\Delta G_{Hbond} \sim 0.6$ kcal mol$^{-1}$, the insertion of both helices will be favorable, whereas if $\Delta G_{Hbond} \sim 2$ kcal mol$^{-1}$, the insertion of only the polyleucine helix will be favorable. In general, whether or not a particular 20 AA segment of a MP is stable as an independent TM structure will depend on the net free energy contribution of the polar and nonpolar side chains relative to the contributions of $\Delta G_{Hbond}$. The detailed energetics will, however, also depend on contributions arising from the properties of the lipid bilayer, so-called bilayer effects, discussed below.

A precise number for $\Delta G_{Hbond}$ will greatly improve the accuracy of hydropathy plots because it determines the so-called decision threshold for TM helix prediction in hydropathy plot analyses (163). Except for two related scales (174, 179) discussed below, all hydrophobicity scales are based on measurements (41), estimates (77), or guesses (39) of side chain hydrophobicities alone. Consequently, because side chain hydropathy plots do not include peptide bond contributions, a peak may or may not indicate a true TM segment. That is, a peak can be correctly interpreted in an absolute thermodynamic sense only if the backbone contribution to partitioning is accounted for in the hydropathy plot.

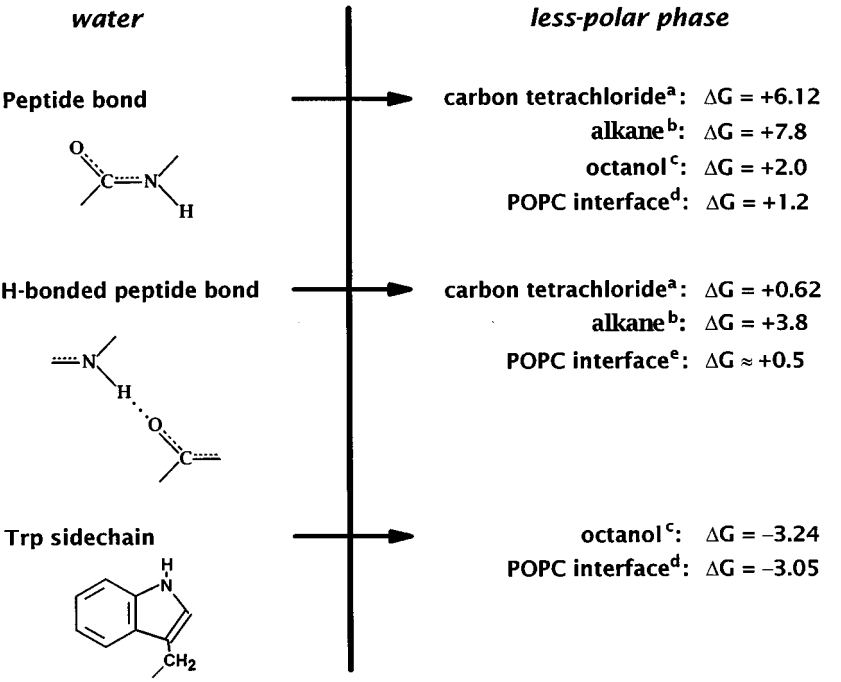


*Figure 3* Summary of the energies of peptide bond partitioning between water and nonpolar phases (kcal/mol). The cost of partitioning non-hydrogen-bonded peptide bonds into completely apolar phases is very high but is lower for partitioning into octanol or into the interface of palmitoyloleoylphosphocholine (POPC) bilayers. The cost of partitioning is dramatically reduced in all cases when peptide bonds participate in hydrogen bonds. This reduction is a major driving force for the formation of secondary structure in membranes and their interfaces. The free energy reduction associated with the partitioning of the most hydrophobic amino acid side chain, tryptophan, is too small to compensate for the cost of partitioning non-H-bonded peptide bonds. Therefore, a TM polypeptide segment composed of nonpolar amino acids can traverse the membrane only if there is complete backbone-backbone hydrogen bonding, as in $\alpha$-helices or $\beta$-barrels (Figure 1). The free energies are from (*a*) Roseman (130), (*b*) Ben-Tal et al (10), (*c*) Wimley et al (174), (*d*) Wimley & White (179), and (*e*) Wimley et al (176) and Ladokhin & White (78).

## *Four-Step Thermodynamic Model for Membrane Protein Folding*

If an MP is at thermodynamic equilibrium, one can think of its folding and stability in terms of thermodynamic models that need not mirror the biological assembly process. Such models are nevertheless important for the design of biological experiments because they describe the thermodynamic context within which biological processes must proceed. These processes have evolved to take useful advantage of thermodynamic equilibrium states by either regulating the heights of barriers separating such states or by using metabolic energy to work against them.

Jacobs & White (61) proposed a three-step thermodynamic model for protein folding (interfacial partitioning, interfacial folding, and insertion) based on structural and thermodynamic measurements of the partitioning of small hydrophobic peptides and the so-called helical hairpin insertion model (38). An essential feature of their model, subsequently supported by several theoretical studies (7, 98), was that the bilayer interface provided a free energy well for initial binding and folding of hydrophobic peptides. At about the same time, Popot & Engelman (113, 114) proposed a two-stage model for the assembly of $\alpha$-helical proteins in which the helices are first "established" across the membrane and then assemble into functional structures. The idea for this model came from a series of experiments that demonstrated that isolated fragments of bR in lipid bilayers can reassemble spontaneously into a fully functional form (114), consistent with the native protein residing in a free energy minimum. Combined, these two lines of thought represent a four-step thermodynamic cycle (Figure 4). The four steps, partitioning, folding, insertion, and association, can proceed along an interfacial path, a water path, or a combination of the two. Determination of the free energies ($\Delta G$) for each step along a path allows thermodynamic stabilities to be computed.

The four-step model is useful for both constitutive and nonconstitutive MPs. For nonconstitutive MPs, the steps progressing from left to right describe the energetics of the natural folding process (see the lower panel of Figure 2), whereas for constitutive MPs, the steps progressing from right to left describe "unfolding." Besides providing a useful thermodynamic scheme, the four-step model summarizes the types of experiments on MP folding that are being pursued in several laboratories.

## *Energetic Components of Partitioning*

One way to obtain the free energy changes of the four-step model is to measure the partitioning of peptides and proteins between the aqueous and membrane phases. The primary causes of favorable partitioning of a peptide or protein

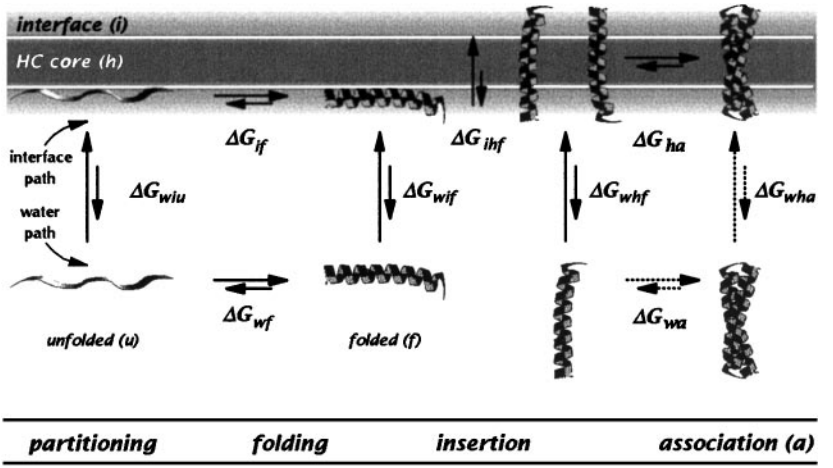


*Figure 4* A four-step thermodynamic cycle for describing the energetics of the partitioning, folding, insertion, and association of an $\alpha$-helix. The process can follow an interfacial path, a water path, or a combination of the two. Studies of folding along the interfacial path are experimentally more tractable (168). The $\Delta G$ symbols indicate standard transfer free energies. The subscript terminology indicates a specific step in the cycle. The subscript letters are defined as follows: $i$ = interface, $h$ = hydrocarbon core, $u$ = unfolded, $f$ = folded, and $a$ = association. With these definitions, for example, the standard free energy of transfer from water to interface of a folded peptide would by $\Delta G_{wif}$.

from water into a membrane are nonpolar (*np*) interactions, due to expulsion of nonpolar compounds from water (hydrophobic effect), and electrostatic (*qE*) attraction between basic amino acid residues and anionic lipids. Upon binding to the membrane, the peptide can change its conformation (*con*) and its motional degrees of freedom due to immobilization (*imm*) in the membrane. In addition, there can be electrostatic (*elc*) effects arising from differences in the dielectric constants of the water and membrane related to the cost of partitioning H-bonded peptide bonds (7). Finally, the partitioning of the peptide can perturb the lipid (*lip*). The standard transfer free energy, $\Delta G^0$, associated with partitioning can be decomposed into a sum of contributions from the various effects (6, 7, 61, 63):

$$\Delta G^0 = \Delta G^0_{np} + \Delta G^0_{elc} + \Delta G^0_{qE} + \Delta G^0_{con} + \Delta G^0_{imm} + \Delta G^0_{lip}. \qquad 1a.$$

Because the first two terms are related to changes in the solvation of the protein upon partitioning, Ben-Tal et al (7) suggest defining a solvation free energy $\Delta G^0_{solv} = \Delta G^0_{np} + \Delta G^0_{elc}$ so that

$$\Delta G^0 = \Delta G^0_{solv} + \Delta G^0_{qE} + \Delta G^0_{con} + \Delta G^0_{imm} + \Delta G^0_{lip}. \qquad 1b.$$

Equation 1 is useful for two reasons. First, it allows the possibility of computing $\Delta G^0$ from first principles if the contributions from each term can be calculated individually. The computation of $\Delta G^0_{qE}$ has been discussed extensively by several authors (9, 136, 148) and approaches for calculating $\Delta G^0_{elc}$, $\Delta G^0_{con}$, $\Delta G^0_{imm}$, and $\Delta G^0_{lip}$ have been discussed in detail by Honig and his colleagues (6, 7) and, earlier, by Jähnig (62). Second, and more pragmatically, when partitioning is driven primarily by the hydrophobic effect, Equation 1 allows membrane partitioning to be considered in the context of bulk-phase partitioning. For simple nonpolar solutes, the desolvation free energy arising from the hydrophobic effect (43, 122, 146) is given by

$$\Delta G^0_{np} = \sigma \cdot A, \qquad 2.$$

where $A$ is the solute's accessible surface area in water and $\sigma$ the solvation parameter, estimated to be about $-20$ to $-25$ cal mol$^{-1}$ Å$^{-2}$ for water-to-hydrocarbon transfer [(23, 122, 129, 174), but see below]. For uncharged molecules ($\Delta G^0_{qE} = 0$), Equation 1b may be written as

$$\Delta G^0 = \Delta G^0_{solv} + \Delta G^0_{bilayer}, \qquad 3.$$

where $\Delta G^0_{bilayer} = \Delta G^0_{con} + \Delta G^0_{imm} + \Delta G^0_{lip}$ represents the contribution of bilayer effects (178) to the partitioning process. The conformational and immobilization components are included because they arise specifically from the association of the peptide with the bilayer. These effects, sometimes called the nonclassical hydrophobic effect (138), are significant for even simple nonpolar molecules. For the transfer of *n*-hexane from water to an alkane phase at 25°C, for example, $\Delta G^0 = -7.74$ kcal mol$^{-1}$, whereas for partitioning into dioleoylphosphocholine bilayers $\Delta G^0 = -5.77$ kcal mol$^{-1}$ on a per acyl-chain basis (140). Thus, $\Delta G^0_{bilayer} = 1.97$ kcal mol$^{-1}$, which is a very significant effect. This simple case demonstrates that membrane partitioning cannot be reliably predicted on the basis of bulk-phase partitioning. Other examples of bilayer-effect deviations are discussed in the section on The Bilayer Milieu.

## *Standard Transfer Free Energies*

Difficulties can arise when transfer free energy data from different laboratories are compared, because different standard states for the transfers are used. Although the preferential association of a solute with the lipid bilayer is frequently treated as macromolecule binding-site problem, the simplest and most rigorous approach is to treat the association as simple partitioning, and to use mole-fraction partition coefficients in the computation of standard transfer free

energies. Figure 5 summarizes various methods of calculating these free energies based on rigorous discussions of several authors (6, 7, 62, 112). Experimental methods for determining partition coefficients have been reviewed in detail (169).

Considerable controversy exists regarding the preferred system of units for calculating free energies, concerned primarily with possible corrections to account for size differences between solutes and solvents, the so-called the Flory-Huggins correction (reviewed in 20). Because water molecules are so small compared to lipid molecules, the size correction can be substantial in bilayer partitioning (167). One important consequence of the size correction is that the nonpolar solvation parameter (Equation 2) is about $-45$ kcal mol$^{-1}$ rather than $-25$ kcal mol$^{-1}$ (34, 139). The controversy revolves around the computation of the so-called cratic entropy. Chan & Dill (20) have given a lucid and detailed account of the issues. The best course, for now, is to use mole fraction partition coefficients for computing free energies (Figure 5).

## THE BILAYER MILIEU

### *Structure of Fluid Lipid Bilayers*

A molecular interpretation of standard free energies of transfer requires experimental knowledge of the structure of the membrane bilayer, the transbilayer location of bound peptides, the structures the peptides adopt, and the changes that occur in the bilayer structure as a result of partitioning. Because cellular membranes must be in a fluid state for normal cell function, it is the structure of fluid ($L_\alpha$-phase) bilayers that is relevant to understanding the interactions of peptides in molecular detail. Unfortunately, the high thermal disorder of fluid bilayers precludes atomic-resolution three-dimensional crystallographic images. Useful structural information can nevertheless be obtained by diffraction methods because multilamellar bilayers (liquid crystals) obtained from phospholipids by dispersal in water or by deposition on surfaces are highly periodic along the bilayer normal. This one-dimensional crystallinity allows the distribution of matter along the bilayer normal to be determined from combined X-ray and neutron diffraction measurements (liquid-crystallography; reviewed in 165, 166). The "structure" of a fluid bilayer that results from such measurements consists of the collection of time-averaged spatial distributions of the principal structural (quasimolecular) groups of the lipid (carbonyls, phosphates, etc) and of water projected onto an axis normal to the bilayer plane (170, 171). The liquid-crystallographic structure of a $L_\alpha$-phase dioleoylphosphatidyl-choline (DOPC) bilayer is shown in Figure 6*A* (172).

Several features of the fluid DOPC structure are important. First, the great amount of thermal disorder is revealed by the widths of the probability densities.

**Mole-Fraction Partition Coefficient**

Standard state: Infinite dilution

$$K_x = x_{bil}/x_w, \quad \Delta G_x^0 = -RT \ln K_x$$

**Molar Partition Coefficient**

Standard state: 1 Molar

$$K_C = C_{bil}/C_w, \quad \Delta G_C^0 = -RT \ln K_C$$

$$K_C = K_x (v_{water}/v_{lipid})$$

$$\Delta G_x^0 = \Delta G_C^0 + RT \ln\left(v_{water}/v_{lipid}\right) = \Delta G_C^0 - 2.2 \text{ kcal mol}^{-1}$$

**Association Constant**

Traditional reference state: 1 Molar

for L + P $\leftrightarrow$ LP: $K_{assoc} = [\text{PL}]/[\text{P}][\text{L}], \quad \Delta G_{assoc} = -RT \ln K_{assoc}$

$$K_{assoc} = K_x/[\text{W}]$$

$$\Delta G_x^0 = \Delta G_{assoc} - RT \ln([W]) = \Delta G_{assoc} - 2.38 \text{ kcal mol}^{-1}$$

Second, the combined thermal thickness of the interfacial regions (defined by the distribution of the waters of hydration) is about equal to the 30 Å thickness of the HC core. The thermal thickness of a single interface (15 Å) can easily accommodate unfolded and folded polypeptide chains, as illustrated schematically in Figure 6*B* by the end-on representation of an $\alpha$-helix with diameter $\sim$10 Å (typical of helices in MPs). In this light, the common cartoons of bilayers that assign a diminutive thickness to the bilayer headgroup/interface region can be seen as misleading. Third, the interfaces are chemically highly heterogeneous; they are rich in possibilities for noncovalent interactions with peptides. Because the interfaces are the sites of first contact, they are especially important in the folding and insertion of nonconstitutive MPs such as toxins (Figure 2). However, they are also important for the folding and stability of constitutive MPs because significant portions of their mass contact the interfaces (Figure 1). The chemical heterogeneity of the interfaces gives rise to a gradient of electrical polarity (Figure 6*B*), calculated from the partial charges of the lipid and water atoms and the quasimolecular group volumes at each position of the bilayer structure. The polarity "profile" for the DOPC bilayer, shown by the heavy line in Figure 6*B* (168), indicates that a molecule moving from water to the hydrocarbon core must experience a dramatic variation in the polarity of its environment. The amphipathic helix represented in Figure 6*B* is located at the mid-point of the steep decent of the polarity gradient.

## *Peculiarities of Bilayer Partitioning: Bilayer Effects*

Because of bilayer effects (Equation 3), the free energy of *n*-hexane partitioning into DOPC bilayers differs significantly from the value for partitioning into a

←

*Figure 5* Various systems used for partition coefficients, association constants, and transfer free energies. Transfer free energy data from different laboratories must be compared with caution because 1. free energies are often calculated (inappropriately) from association constants (units of $M^{-1}$) based on binding site models, and 2. the standard states for the transfers are not always defined clearly. The simplest and most rigorous approach is to treat the association of peptides with membranes as a partitioning rather than a binding-site problem and to use mole-fraction partition coefficients for calculating standard state transfer free energies, $\Delta G^0$. This figure summarizes different systems encountered frequently in the literature and relates them to the mole-fraction system. Conversions of molar and association free energies to mole-fraction standard transfer free energies involve only additive terms. Therefore, differential free energy terms, $\Delta\Delta G_{assoc}$ and $\Delta\Delta G_c^0$, will be identical to $\Delta\Delta G_x^0$. The figure is based on several rigorous discussions of standard transfer free energies presented by several authors (6, 7, 62, 112, 169). All equations assume partitioning from the water (*w*) phase to the bilayer (*bil*) phase. Abbreviations: [*L*], molar concentration of lipid; [*P*], molar concentration of peptide; [*PL*], molar concentration of peptide bound to lipid; [*W*], molar concentration of water (55.3). The molar volumes of lipid and water are $v_{lipid}$ and $v_{water}$, respectively. For the typical phospholipid (178), $v_{lipid} \approx 1300$ Å$^3$, $v_{water} = 30$ Å$^3$.

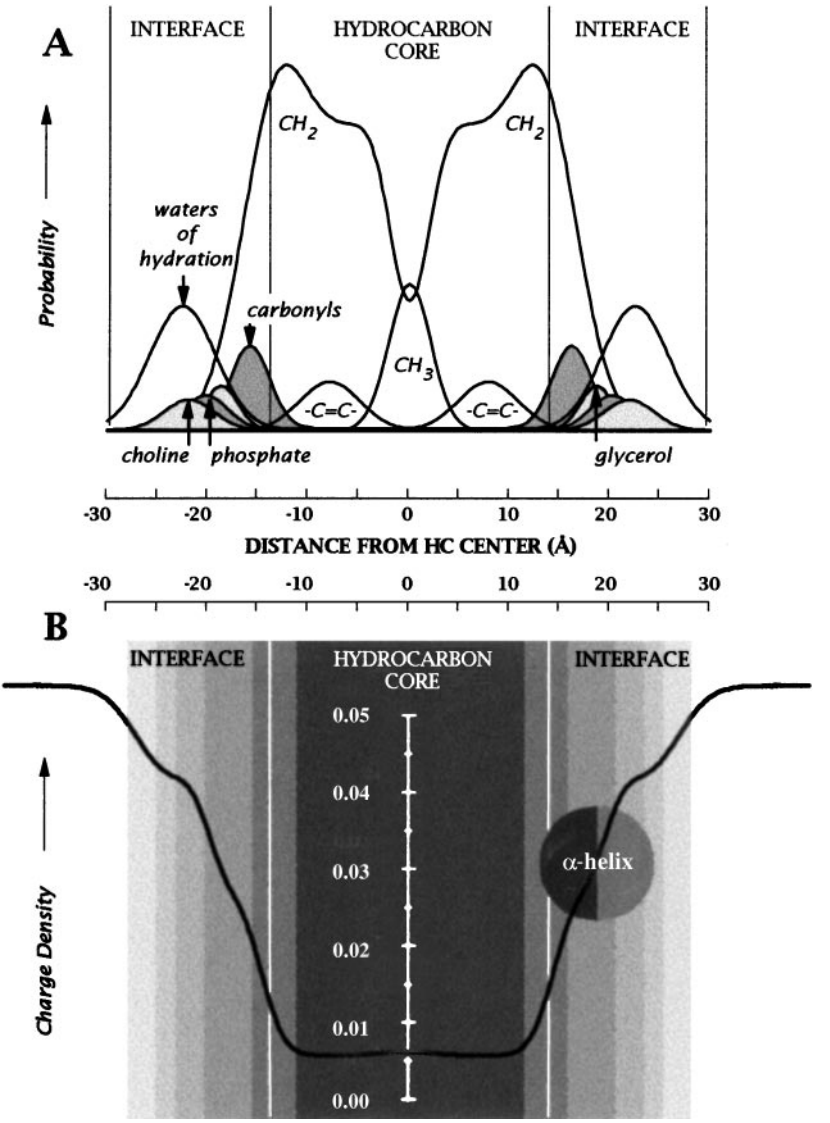
A
INTERFACE
HYDROCARBON CORE
INTERFACE
Probability
CH2
CH2
waters of hydration
carbonyls
CH3
-C=C-
-C=C-
choline
phosphate
glycerol
-30
-20
-10
0
10
20
30
DISTANCE FROM HC CENTER (Å)
B
INTERFACE
HYDROCARBON CORE
INTERFACE
Charge Density
0.05
0.04
0.03
0.02
0.01
0.00
α-helix

bulk alkane phase, as discussed above. These effects, observed for a wide range of solutes (138, 178), demonstrate the peculiarities of bilayer partitioning that must be accounted for in MP folding. For *n*-hexane, the effects are undoubtedly related to its nonuniform transbilayer distribution, shown in Figure 7*A*. Hexane molecules are confined to the region occupied by the acyl chain methyl groups, and NMR studies (60) show that they undergo anisotropic motions related to acyl chain motions. Extensive studies of the thermodynamics of the solubility of a variety of alkanes and their isomers in black lipid membranes (161) showed that the enthalpies and entropies of alkane solubility depend dramatically on the structure of the isomer, including branching and chain length, which suggests that the interaction energies of MP side chains may depend on their TM bilayer positions.

Bilayer effects are not restricted to molecules that reside exclusively in the HC core. Figure 7*B* compares interfacial partitioning of tryptophan analogs into the bilayer interface with partitioning into bulk cyclohexane. In all cases, the interfacial transfer free energies differ from the cyclohexane values and are characterized by dramatically favorable enthalpies, a hallmark of bilayer effects (178). A study of the partitioning of the 25-residue COX IVp peptide into bilayer interfaces also disclosed bilayer effects (131). The interfacial partitioning of the

←

*Figure 6* The structure of a fluid liquid-crystalline bilayer and its polarity profile. (*A*) The structure of a dioleoylphosphocholine (DOPC) bilayer determined by the joint refinement of X-ray and neutron diffraction data (172). The "structure" consists of the time-averaged distributions of the principal (quasi-molecular) structural groups of the lipid projected onto an axis normal to the bilayer plane. The areas of the Gaussian distributions equal the number of structural groups represented by the Gaussians (1 phosphate, 2 carbonyls, etc); the distributions therefore represent the probability of finding a structural group at a particular location. The interfaces of the bilayer are defined as the regions occupied by the headgroup's water of hydration. Although this structural image was obtained at low hydration, 5.4 waters per lipid, recent work demonstrates that the overall structure changes in relatively minor ways as the water content is increased (52). The figure is modified from that of White (163). (*B*) Polarity profile (*heavy line*) derived from the group distributions of panel *A* (168). The "polarity" of the membrane is described by the absolute partial-charge densities of the quasimolecular groups. Group partial-charge densities were calculated for each quasimolecular group using the atomic partial charges of Charifson et al (22) and the group volumes given by Wiener & White (172). The polarity profile is obtained from the average charge density, calculated by weighting the group charge densities by the number density and group volume at each position (168). Also shown is the schematic cross section, drawn to scale, of the amphipathic $\alpha$-helical peptide 18A whose position has been determined by X-ray diffraction (K Hristova, WC Wimley, VK Mishra, GM Anantharamiah, JP Segrest & SH White, in preparation). Note that its location is at the steepest point of the polarity gradient of the interface where the lipid polar groups give way to the hydrocarbon chains. This gradient is symbolized by *gradations of gray*. The representations of the fluid bilayer in Figures 2 and 4 are based on this symbolic scheme. The polarity profile is redrawn from Wimley & White (168).

**A**

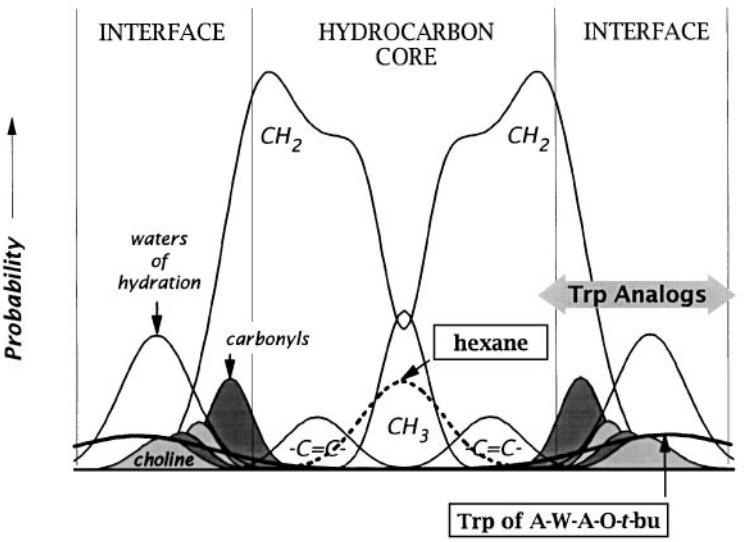


**B**


| Solute | Solvent | ΔG (kcal/mol) | ΔH (kcal/mol) | ΔS cal/(mol·K) |
|---|---|---|---|---|
| *N-methylindole* | *cyclohexane* | *-7.16* | *+1.11* | *+27.7* |
| | *bilayer* | *-8.08* | *-3.45* | *+15.5* |
| *3-methylindole* | *cyclohexane* | *-5.95* | *+2.42* | *+28.1* |
| | *bilayer* | *-8.60* | *-5.42* | *+10.7* |
| *indole* | *cyclohexane* | *-4.36* | *+2.56* | *+23.3* |
| | *bilayer* | *-7.61* | *-5.37* | *+7.5* |

tripeptides Ala-X-Ala-*O-tert*-butyl (X = Gly, Ala, Leu, Phe, Trp) permitted bilayer effects to be examined in the context of Equation 3 (61). A plot of the tripeptide transfer free energies against $\Delta G^0_{np}$ revealed that the solvation parameter $\sigma$ (Equation 2) has an apparent value of $-12.4$, rather than the value of $-20$ to $-25$ cal mol$^{-1}$ Å$^{-2}$ expected for bulk-phase partitioning. Studies of pentapeptides (179), discussed below, suggest that the lowered value is related to $\Delta G^0_{elc}$ in Equation 1. As discussed elsewhere (175, 179), a simple, but probably incomplete, explanation may be that the average dielectric coefficient of the interface is intermediate between that of water and octanol, perhaps ~18.

A persistent result of diffraction and other studies of peptides interacting with bilayers is that bilayer thickness is generally affected. For TM $\alpha$-helical peptides, bilayers either thicken or thin, depending on the length of the helix relative to the thickness of the hydrocarbon (33, 102), in order to reduce so-called hydrophobic mismatch (105), which can modify lipid phase behavior (reviewed in 104, 106). Bilayers are not passive receptacles for proteins. They adapt structurally to TM helices in order to minimize the free energy of the system. Interfacially bound peptides also have a general tendency to cause thickness decreases, even at very low peptide:lipid (P:L) ratios (47, 61). The dependence of the decrease on P:L has been modeled (47) with a mean-field theory based on bilayer compressibility and bending moduli. There is evidence indicating that bilayer bending rigidity is important in the refolding of bacteriorhodopsin (15). Theories based on compressibility and bending moduli provide a connection to bilayer effects via $\Delta G^0_{lip}$ and $\Delta G^0_{imm}$ (see 6, 105). These results imply that a bilayer containing peptides differs thermodynamically in some fundamental way from the "neat" bilayer. Indeed, Morrow et al (103) concluded from an analysis of the phase behavior of lipids in the presence of TM helices that the peptide "influences the transition thermodynamics for the bilayer as a whole" (p. 5405).

←

*Figure 7* The transbilayer location of several hydrophobic compounds in a fluid DOPC bilayer and thermodynamic parameters describing the partitioning of tryptophan analogs. (*A*) The structure of the DOPC bilayer is that of Figure 6*A*. The transbilayer distributions of *n*-hexane (164) and the Trp of Ala-Trp-Ala-*O-tert*-butyl (61) were determined by neutron diffraction. Also shown is the location of the Trp analogs of *panel B* determined using NMR methods (182) (*broad double arrow*). Hexane is located in the center of the bilayer, as anticipated from electrical studies of black lipid membranes (162), whereas Trp and its analogs are located in the interface. This shows that the preference of Trp residues of membrane proteins for membrane surfaces (Figure 1) probably arises from favorable interactions of aromatic groups with the interface. (*B*) The thermodynamic parameters associated with the partitioning of Trp analogs from water to cyclohexane (177) and to phosphocholine bilayer interfaces (178). The data show that cyclohexane partitioning is driven mostly by entropy due to the hydrophobic effect, whereas interfacial partitioning also has a very favorable enthalpic component. This provides further support for the idea of highly favorable interactions of aromatic residues with the bilayer interface.

### *Interfacial Partitioning and Aromaticity*

Neutron diffraction studies of the tripeptide Ala-Trp($d_5$)-Ala-*O-tert*-butyl in DOPC bilayers (61), summarized in Figure 7*A*, provided the first direct evidence of a physical basis for the strong preference of the aromatic amino acids of MPs for membrane surfaces (Figure 1). Remarkably, the Trp distribution was found to be approximately the same as that of the water—the Trp prefers the headgroup region, not the HC core. This was surprising because it is generally assumed that Trp interacts with bilayers in an amphipathic manner (134). That is, it should bury itself in the hydrocarbon core with its imino group H-bonded to the phospholipid carbonyls and water.

A recent detailed NMR study (182) of several Trp analogs (Figure 7*B*) demonstrates that the Trp distribution observed by neutron diffraction is a direct result of the properties of the indole ring itself rather than a peculiarity of the tripeptide. All three of the Trp analogs of Figure 7*B* along with indene (NH of indole replaced by $CH_2$) were found to be confined exclusively to the vicinity of the glycerol group of the lipids of palmitoyloleoylphosphocholine (POPC) bilayers, despite marked differences in dipole moment and H-bonding ability. Another NMR (110) study of indole and 3-methylindole in ester- and ether-linked phospholipids also demonstrated that H-bonding is not a determinant of the interfacial locations. The exact physical basis for the Trp interfacial preference is uncertain, but it appears to be related to the flat, rigid shapes of the analogs and their $\pi$ electronic structures and associated quadrupolar moments (aromaticity). Yau et al (182) concluded from their NMR measurements that the interfacial preference of tryptophan is due to a balance of forces: the hydrophobic effect tends to drive it out of water, complex electrostatic interactions favor its residence in the hydrated headgroup region, and cohesive repulsion forces disfavor its presence in the HC core.

## ENERGETICS OF PEPTIDES IN BILAYER INTERFACES

The properties of the bilayer milieu show clearly that the bilayer interface is distinct both structurally and chemically. Because significant portions of MPs reside in this complex region (Figure 1), the energetics of peptide interactions there are important to understand. The very strong tendency of bilayer interfaces to promote secondary structure in membrane active peptides (78, 176) provides the simplest evidence of the importance of these energetics. Besides being inherently important, studies of peptides at interfaces form the basis for a bootstrap strategy for determining the free energy cost $\Delta G_{whf}$ (Figure 4) for establishing an $\alpha$-helix across the bilayer—a measurement fraught with

problems when done directly (see below). This strategy is discussed elsewhere (168).

### *Whole-Residue Hydrophobicity Scales*

An hydrophobicity scale, composed of experimentally determined transfer free energies for each amino acid, is an essential first step for studies of water-to-interface transfer free energies, $\Delta G_{wiu}$, of unfolded peptide chains (Figure 4). The most important feature of a practical scale is the inclusion of contributions of the peptide bonds, for the obvious reason that whole residues, not just side chains, partition into the interface. That is, it must be a whole-residue scale. Wimley & White (179) determined such a scale for POPC bilayer interfaces using two families of peptides: host-guest pentapeptides of the form AcWL-X-LL, for determining side chain hydrophobicities, and the homologous series $AcWL_m$ ($m = 1 \ldots 6$), for determining peptide bond hydrophobicity. In order to compare bilayer partitioning with bulk-phase partitioning, these families were also used to establish a whole-residue hydrophobicity scale for partitioning into *n*-octanol (168, 174). As shown here, for the first time, the use of the two whole-residues scales together appears to be of value in hydropathy plot analyses.

The transfer free energies determined using the two peptide families are summarized in Figure 8 (168, 174, 179). A comparison of the partitioning of the $AcWL_m$ peptides into the POPC bilayer interface and into octanol (Figure 8*A*) leads to three important conclusions. First, the transfer free energies appear to be additive, as shown by the best-fit straight line through the points. This additivity, confirmed by plots of $\Delta G$ against $m$ for both host phases (174, 179), is an essential criterion for computing the $\Delta G_{wiu}$ of an arbitrary peptide sequence. Second, the intercept of the straight line is negative ($-2.5$ kcal mol$^{-1}$), rather than positive. This is contrary to the expectation (7, 63) that the reduction in dimensionality accompanying transfer from water to bilayer, $\Delta G_{imm} + \Delta G_{lip}$ in Equation 1, is highly unfavorable. Third, the slope of the straight line has a value of 0.49. This confirms that the interfacial solvation parameter $\sigma$ (Equation 2) for POPC is about one half the value observed for bulk-phase partitioning.

Figure 8*B* shows that a slope 0.49 also broadly describes the relationship between side chain hydrophobicity values for the interface and octanol. Because charged and polar as well as nonpolar residues are included, a reduced interfacial solvation parameter appears to be a general property of the interface. This implies that $\Delta G_{elc}$ in Equation 1 may be responsible. Figure 8*B* also shows that the aromatic residues, with very favorable free energies, and the charged residues, with very unfavorable free energies, dominate the free energy of partitioning. That the aromatics are exceptionally favorable is consistent with the observations on indole partitioning (see above). Combining the results from $AcWL_m$ and AcWL-X-LL partitioning leads to values for the partitioning

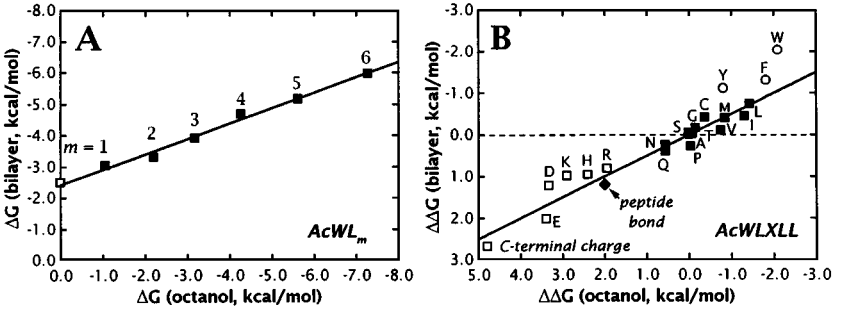


## C Whole-Residue Hydrophobicity Scales

free energies of transfer $\Delta G$ from water to POPC interface (*wif*) and to *n*-octanol (*woct*)

| Amino Acid | *Interface Scale* $\Delta G_{wif}$ (kcal/mol) | *Octanol Scale* $\Delta G_{woct}$ (kcal/mol) |
|---|---|---|
| Ala | 0.17 ± 0.06 | 0.50 ± 0.12 |
| $Arg^+$ | 0.81 ± 0.11 | 1.81 ± 0.13 |
| Asn | 0.42 ± 0.06 | 0.85 ± 0.12 |
| $Asp^-$ | 1.23 ± 0.07 | 3.64 ± 0.17 |
| $Asp^0$ | −0.07 ± 0.11 | 0.43 ± 0.13 |
| Cys | −0.24 ± 0.06 | −0.02 ± 0.13 |
| Gln | 0.58 ± 0.08 | 0.77 ± 0.12 |
| $Glu^-$ | 2.02 ± 0.11 | 3.63 ± 0.18 |
| $Glu^0$ | -0.01 ± 0.15 | 0.11 ± 0.12 |
| Gly | 0.01 ± 0.05 | 1.15 ± 0.11 |
| $His^+$ | 0.96 ± 0.12 | 2.33 ± 0.11 |
| $His^0$ | 0.17 ± 0.06 | 0.11 ± 0.11 |
| Ile | −0.31 ± 0.06 | −1.12 ± 0.11 |
| Leu | −0.56 ± 0.04 | −1.25 ± 0.11 |
| $Lys^+$ | 0.99 ± 0.11 | 2.80 ± 0.11 |
| Met | −0.23 ± 0.06 | −0.67 ± 0.11 |
| Phe | −1.13 ± 0.05 | −1.71 ± 0.11 |
| Pro | 0.45 ± 0.12 | 0.14 ± 0.11 |
| Ser | 0.13 ± 0.08 | 0.46 ± 0.11 |
| Thr | 0.14 ± 0.06 | 0.25 ± 0.11 |
| Trp | −1.85 ± 0.06 | −2.09 ± 0.11 |
| Tyr | −0.94 ± 0.06 | −0.71 ± 0.11 |
| Val | 0.07 ± 0.05 | −0.46 ± 0.11 |

of the peptide bond into octanol and the POPC bilayer interface of +2.0 and +1.2 kcal mol$^{-1}$, respectively (174, 179). These values, included in Figure 8*B*, show that the peptide bond is as costly to partition as the charged side chains! The peptide bond thus has a dominant effect on interface partitioning, just as it does for HC core partitioning. Combining the peptide-bond free energies with the side chain free energies yields whole-residue hydrophobicity scales for both the POPC interface and octanol. These scales are shown in Figure 8*C* (168).

Earlier discussion emphasized the importance of including peptide bond free energy contributions ($\Delta G_{Hbond}$) in hydropathy plots of MPs, because they determine the decision level for TM helix selection. Estimates for $\Delta G_{Hbond}$ as part of an $\alpha$-helix range from +0.6 to +2.1 kcal mol$^{-1}$, as discussed earlier. The contribution of the –$CH_2$-CONH– glycyl unit to the partitioning of whole residues into *n*-octanol (174) is +1.15 kcal mol$^{-1}$, a value that falls squarely in the middle of the expected range for $\Delta G_{Hbond}$. The whole-residue octanol scale may therefore be useful for identifying TM segments in hydropathy plots of MPs. This idea is supported by the whole-residue octanol-scale hydropathy plot for the L-subunit of the photosynthetic reaction center of *Rhodobacter sphaeroides* shown in Figure 9 (*light solid line*). Because TM segments should generally prefer the bilayer rather than water, one would also expect the whole-residue interfacial scale to identify TM segments. This conclusion is supported by Figure 9 (*dotted line*). In addition, however, one would expect true TM segments to have more favorable free energies on the octanol scale than on the interfacial scale. Figure 9 (*heavy solid line*) shows that this expectation

←

*Figure 8* Comparisons of the partitioning of peptides into bilayer interfaces with their partitioning into octanol and a table of whole-residue hydrophobicity scales. All free energies are in kcal mol$^{-1}$ calculated using mole-fraction units. The whole-residue hydrophobicity scales show promise of being useful in hydropathy plots (Figure 9). (*A*) Comparison of water-to-bilayer partitioning with water-to-octanol partitioning for the peptides $AcWL_m$ with $m = 1 - 6$. The *solid line* is a linear regression of the bilayer data against the octanol data. The slope is $0.49 \pm 0.04$ and the intercept $-2.40 \pm 0.16$ kcal/mol. [Based on (179)]. (*B*) Comparisons of water-to-bilayer partitioning with water-to-octanol partitioning for the peptides AcWL-X-LL where X is one of the 20 natural amino acids. The *solid line* has the slope of 0.49 determined in A [Based on (179)]. (*C*) Table of whole-residue free energies of transfer $\Delta G$ from water to POPC interface (179) and to *n*-octanol (174) [based on (168)]. The values for $\Delta G_{wif}$ are taken directly from Reference (179). The values of $\Delta G_{woct}$ are computed from data in Reference (174) by adding the solvation energy $\Delta G_{glycyl}$ of the –$CH_2$-CONH– unit [$-1.15 \pm 0.11$ kcal/mol (174)] to the occlusion-corrected side chain solvation energies $\Delta G_X^{cor}$ found in Table 2 of (174). For both $\Delta G_{wif}$ and $\Delta G_{woct}$, the signs have been reversed relative to those of the original publications to reflect free energies of transfer from the water phase.

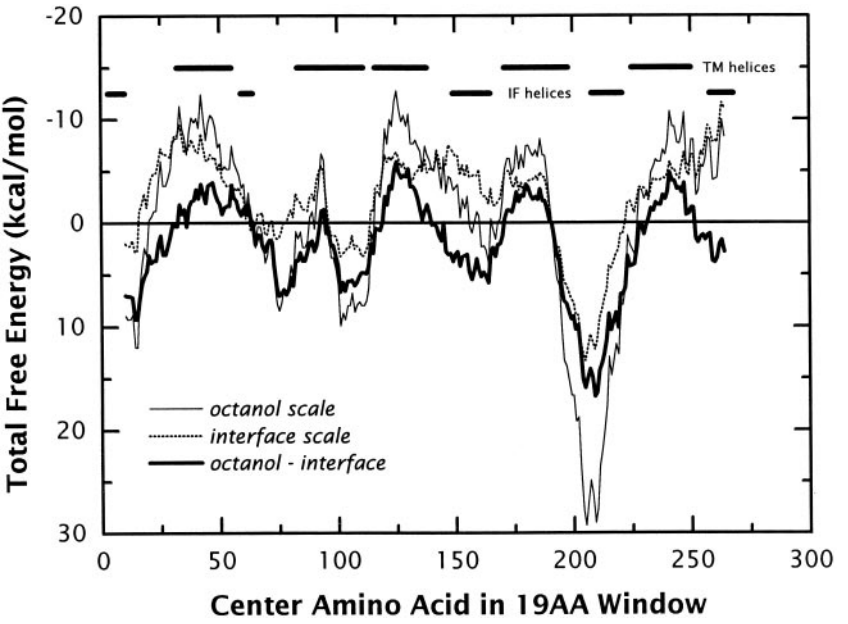
-20
-10
0
10
20
30
Total Free Energy (kcal/mol)
TM helices
IF helices
octanol scale
interface scale
octanol - interface
0
50
100
150
200
250
300
Center Amino Acid in 19AA Window

is also met, at least for the L-subunit: The hydropathy plot constructed using $\Delta G_{woct} - \Delta G_{wif}$ (Figure 8*C*) shows favorable peaks on the absolute scale that correspond to the known TM helices. Significantly, the maxima have more restricted sequence-ranges than seen with either of the scales alone and thus identify with less ambiguity the positions of the TM helices. These results make perfect sense: TM helices will choose to be associated with the membrane rather than the water and will prefer a TM location rather than a surface one. Were this not true, MPs would not be stably buried in the membrane.

### *Bilayer-Induced Secondary Structure Formation*

The germinal work of Kaiser & Kézdy (68) first demonstrated that the partitioning of peptides and small proteins into membranes often induces the formation of secondary structure, a process conveniently described as partitioning-folding coupling (179). For that to be true, it must also be true that the overall free energy cost of partitioning the folded peptide is significantly lower than for the unfolded peptide (61). This simple idea focuses attention on $\Delta G_{if}$ (Figure 4) and suggests the possibility of quantitative rules for the design of peptides with specified partition coefficients and secondary structure propensities.

Given their observation (above) that it is energetically costly to partition peptide bonds into the interface, Wimley & White (179) hypothesized that participation of peptide bonds in H-bonding would dramatically reduce a peptide's partitioning free energy and thus cause partitioning-folding coupling. This hypothesis is borne out by two recent measurements of the energetics of $\alpha$-helix (78) and $\beta$-sheet (176) formation, summarized in Figure 10. These

←

*Figure 9* Hydropathy plots of the L-subunit of the photosynthetic reaction center of *Rhodobacter sphaeroides* determined using whole-residue hydrophobicity scales (Figure 8). These plots are on an absolute scale and include the contributions of the peptide bonds to partitioning. The *heavy horizontal lines* are the known sequence locations of transmembrane (TM) and interfacial (IF) $\alpha$-helices determined by X-ray crystallography (183). Total free energy is the sum of the hydrophobicity scale values in a window of length 19 amino acids. This plot shows that both the octanol and interfacial hydrophobicity scales of Figure 8 (*light solid and dotted lines*, respectively) successfully locate known TM helices. More important, a plot based on the difference of the octanol and interfacial scales (*heavy solid line*) also successfully predicts the locations, but more nearly coincides with the positions of the helices. Both the octanol and interfacial scales seem to indicate those regions of the sequence that prefer to be associated with membrane rather than water. The difference-scale plot suggests that the regions of the sequence that prefer to be across the membrane can be distinguished from those that prefer associating with the interface. This makes sense: TM helices will choose to be associated with the membrane rather than the water and will prefer a TM location rather than a surface one. Were this not true, membrane proteins would not be stably buried in the membrane.

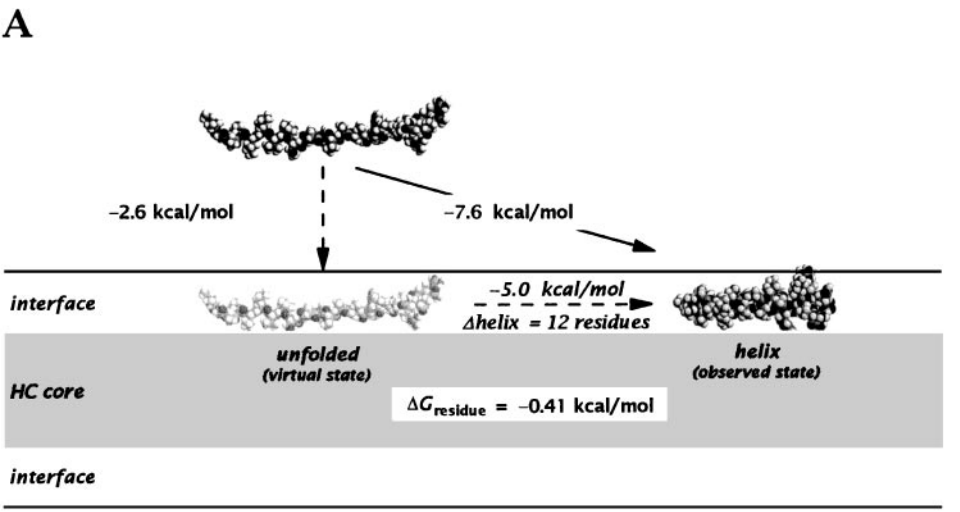
A
−2.6 kcal/mol
−7.6 kcal/mol
interface
−5.0 kcal/mol
Δhelix = 12 residues
unfolded
(virtual state)
helix
(observed state)
HC core
ΔG residue = −0.41 kcal/mol
interface

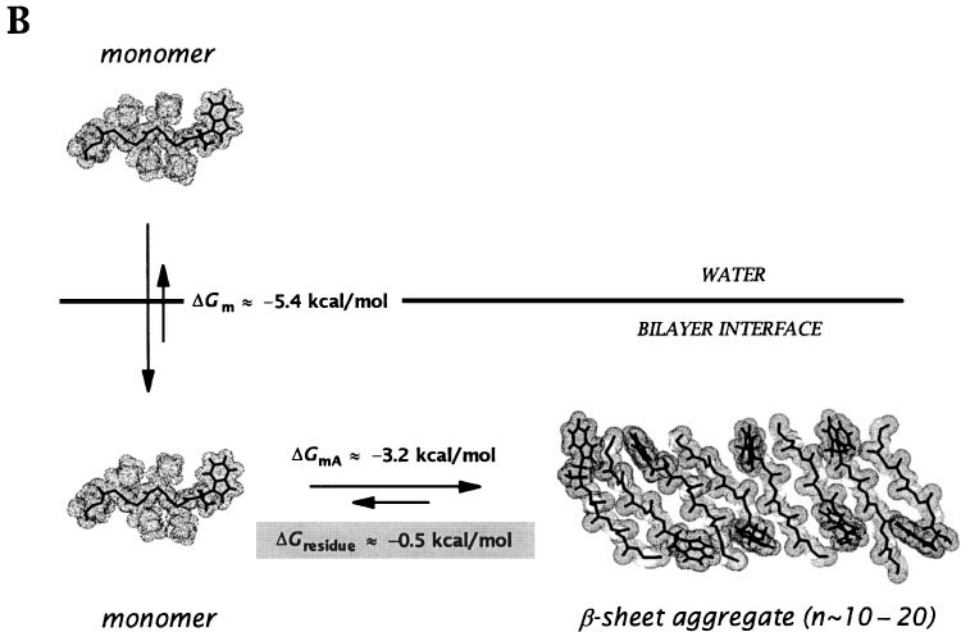
B
monomer
ΔG m ≈ −5.4 kcal/mol
WATER
BILAYER INTERFACE
ΔG mA ≈ −3.2 kcal/mol
ΔG residue ≈ −0.5 kcal/mol
monomer
β-sheet aggregate (n~10 – 20)

measurements suggest that the per-residue free energy reduction, $\Delta G_{residue}$, accompanying secondary structure formation is typically $-0.5$ kcal mol$^{-1}$. This value allows one to estimate $\Delta G_{if}$ from $\Delta G_{wiu}$ (Figure 4).

Although the primary driving force for partitioning-folding coupling arises from the free energy reduction associated with H-bonding, $\Delta G_{residue}$ is probably not due to this effect alone. Other interactions must also contribute, including the effects of folding/assembly entropy, side-chain packing, relative exposure of side-chains to membrane and water, and the depth of membrane penetration of secondary structure units. The depth of penetration of helices is likely to be strongly affected by the hydrophobicity-hydrophilicity pattern of the peptide sequence that defines the hydrophobic moment (37). The location of the 18 Å amphipathic helix shown in Figure 6*B* is consistent with this idea. The general amino acid composition of a peptide also appears to be important (14, 30, 86), and there is evidence of important connections between helicity, hydrophobic moment, and lipid charge on the membrane activity of amphipathic helices (29, 173). Jacobs & White (61) proposed the existence of a strong free energy gradient for driving peptides into the HC core due to the difference in the nonpolar solvation parameters (Equation 2) between the interface ($-12$ kcal mol$^{-1}$ Å$^{-2}$) and the HC core ($-25$ kcal mol$^{-1}$ Å$^{-2}$).

←

*Figure 10* Summaries of the energetics of partitioning-folding coupling for $\alpha$-helix formation by melittin and $\beta$-sheet formation by the hexapeptide $AcWL_5$. (*A*) Partitioning and folding of melittin into POPC interfaces [based on (78)]. Melittin is monomeric at low concentrations in aqueous solution where it exists in a disordered state with low $\alpha$-helical content. When bilayer vesicles are titrated into a melittin solution, however, the fraction of melittin partitioned into the vesicles and the average melittin helicity increase concomitantly (152, 169), indicating bilayer induction of secondary structure. The presence of a very distinct isodichroic point in the CD spectra (152, 169) demonstrates a two-state transition in which there are only two populated states: monomeric melittin in water with low helicity and membrane-bound melittin with high helicity. Because of the very tight coupling of folding to partitioning, the energetics of partitioning unfolded melittin are not accessible directly. To access these energetics, the virtual unfolded bound state of melittin is emulated by a melittin diastereomer containing four D-amino acids that inhibit folding (107). The free energies of transfer $\Delta G$ of diastereomeric melittin and melittin were determined from mole-fraction partition coefficients and the changes in helicity from CD measurements. (*B*) Summary of the partitioning and aggregation of $AcWL_5$ into phosphocholine bilayer interfaces [based on (176)]. The hexapeptide $AcWL_5$ avidly forms $\beta$-sheet aggregates in a highly cooperative manner upon partitioning into phosphocholine bilayers. Because $AcWL_5$ is strictly monomeric in the aqueous phase, $\beta$-sheet formation is induced by the bilayer. Partitioning and other measurements reveal the details of the aggregation process, which is temperature dependent and reversible (176). The structures of the monomers and aggregate of $AcWL_5$ are shown for illustrative purposes only and should not be taken literally. Here the aggregate is shown as containing 8 monomers; the average aggregate size is actually 10 or greater.

# ENERGETICS OF TRANSMEMBRANE HELIX INSERTION

## *Theoretical Considerations*

The estimates for TM helix-insertion energetics ($\Delta G^0_{whf}$ in Figure 4) presented earlier were based on bulk-phase partitioning data. Correct estimates, however, must take into account all of the terms of Equation 1 because the contribution of $\Delta G^0_{bilayer}$ to partitioning (Equation 3) is expected to be significant. Ignoring $\Delta G^0_{qE}$ and $\Delta G^0_{elc}$ in Equation 1, Jähnig (62) made the first estimates of $\Delta G^0_{whf}$ which included bilayer effects, especially $\Delta G^0_{imm}$ and $\Delta G^0_{lip}$. He argued that $\Delta G^0_{wf}$ (Figure 4) was zero (which seems unlikely) and estimated $\Delta G^0_{np}$ to be $-35$ kcal mol$^{-1}$, equivalent to the desolvation free energy of a 20 AA polyvaline helix. $\Delta G^0_{imm}$ was estimated assuming that it arose from two effects, restriction in the volume of space available to the helix when transferred from free solution to the membrane ($\sim$8 kcal mol$^{-1}$) and restriction in the rotational degrees of freedom upon transfer ($\sim$8 kcal mol$^{-1}$). A helix in the membrane was assumed to order lipid acyl chains in its vicinity at a cost of $\Delta G^0_{lip} \sim 2$ kcal mol$^{-1}$, based on a continuum model for the bilayer. These estimates led to a value of $\Delta G^0$ in Equation 1b of $-17$ kcal mol$^{-1}$, or about one half the value expected from $\Delta G^0_{np}$ alone.

Honig and his colleagues (6, 7) reexamined, corrected, and refined the Jähnig (62) calculation by considering a 20 AA segment of a polyalanine TM helix. In broad terms, they corrected a problem with Jähnig's standard states, introduced and computed $\Delta G^0_{elc}$ to account for the cost of partitioning H-bonded peptide bonds, and revised and refined the estimates of $\Delta G^0_{imm}$ ($\sim$5 kcal mol$^{-1}$) and $\Delta G^0_{lip}$ ($\sim$2.3 kcal mol$^{-1}$). [These two numbers are at odds with the favorable measured value for $\Delta G_{imm} + \Delta G_{lip}$ for the AcWL$_m$ peptides (see above)]. Because the AcWL$_m$ peptides form random coils, the implication for helix insertion it is not clear. They found that $\Delta G^0_{np} = -36$ and $\Delta G^0_{elc} = 25$ kcal mol$^{-1}$, and consequently that $\Delta G^0 = -4$ kcal mol$^{-1}$ (molar partition coefficients, Figure 5). The primary conclusions of their analysis are that (*a*) $\Delta G^0_{lip}$ and $\Delta G^0_{imm}$ are not as unfavorable as the Jähnig estimates and (*b*) the $\Delta G^0_{elc}$ term, not included in Jähnig's analysis (62), makes a dominant contribution to the energetics of insertion. The take-home message that emerges, taking $\Delta G^0_{np}$ as 100%, is that $\Delta G^0_{lip}$ and $\Delta G^0_{imm}$ together could have a 20% effect and $\Delta G^0_{elc}$ a 70% effect on the insertion of a TM $\alpha$-helix.

## *Experimental Measurements*

Examinations of the energetics of the insertion of TM helices have been reported by several groups (5, 54, 101, 142). Moll & Thompson (101) attempted

to measure $\Delta G_{whf}$ along the water path by measuring the partitioning of a 20-residue alanine peptide that was covalently linked to bovine pancreatic trypsin inhibitor (BPTI). Their reported value of about $-5$ kcal mol$^{-1}$ (mole fraction units) is uncertain for three reasons. First, it is not clear whether the measurement was of $\Delta G_{whf}$ or $\Delta G_{whf} + \Delta G_{fw}$ because the helix content of the $Ala_{20}$ peptide was not determined. Second, $Ala_{20}$ alone is unlikely to be soluble as monomer (WC Wimley & SH White, unpublished data), raising the possibility that the $Ala_{20}$ domain may associate noncovalently in some way with the BPTI carrier, further confusing the meaning of the reported free energy. Third, no evidence was presented that the $Ala_{20}$ domain actually crossed the lipid bilayer, was adsorbed only on the surface, or was distributed between surface and TM locations. Despite these uncertainties and in the light of the earlier discussion, $-5$ kcal mol$^{-1}$ ($-3$ kcal mol$^{-1}$ in molar partitioning units) is not an unreasonable value of $\Delta G_{whf}$ for $Ala_{20}$.

Soekarjo et al (142) showed that the insertion of M13 procoat protein into bilayers follows the interfacial path and cleverly determined free energies associated with the process. They found that M13 procoat, containing two putative TM domains, was distributed 80% in the interface and 20% across the bilayer, based on proteinase K digestion experiments. They concluded that $\Delta G_{whf} = -17$ kcal mol$^{-1}$ for the presumed two-helix hairpin and estimated that $\Delta G_{whf} = -14$ kcal mol$^{-1}$ for a single helix (mole fraction units). Although these experiments represent an excellent attempt to measure $\Delta G_{whf}$, they suffer from a failure to determine the secondary structure of procoat in either the aqueous or membrane phases or to establish with certainty that the proteinase-resistant population of procoat was truly across the membrane. Therefore, uncertainty remains about exactly what free energies terms are represented by their value for $\Delta G_{whf}$.

Bechinger (5) examined $\Delta G^0_{ihf}$ (Figure 4) through measurements of the insertion of a Leu-Ala-His peptide [KKLAL$(LA)_2$L**HH**$(LA)_1$**H**$(LA)_1$L**H**$(LA)_2$LKK $\equiv LAH_4$] into oriented POPC multilayers. Using $^{15}$N NMR and pH titration measurements, he determined the fraction of $LAH_4$ oriented across the bilayer relative to $LAH_4$ oriented parallel to the bilayer (in the bilayer interface) as a function of pH after having determined the $pK_a$ of the histidine residues by means of peptides solubilized in dodecylphosphocholine-$d_{38}$ micelles. The fraction in the transbilayer orientation increased from 0 at pH 4 to 1.0 at about pH 7. The energetics of the process were examined by means of the free energy of discharge $\Delta G^0_d$ associated with deprotonation calculated from $\Delta G^0_d = n_i RT \ln r + 2.3RT \sum_i (pK_i - pH)$, where $r$ is the ratio of charged to uncharged side chain species and $n_i$ is the number of titratable side chains of type $i$. Because Bechinger's experiment measures the fraction $f$ in the perpendicular orientation, one can use Equation 1a to show that

$\Delta G^0_{ihf} = \Delta G^0_d + \Delta\Delta G^0_{np} + \Delta\Delta G^0_{elc} + \Delta\Delta G^0_{con} + \Delta\Delta G^0_{imm} + \Delta\Delta G^0_{lip}$. At pH $= 6.1 \pm 0.2$, $\Delta G^0_d = 8.8$ kcal mol$^{-1}$ and $f = 0.5$ so that $\Delta G^0_{ihf} = 0$. Under these circumstances, the discharge term balances all of the other terms in Equation 8. One can reasonably assume that $\Delta\Delta G^0_{con}$ and $\Delta\Delta G^0_{imm}$ are each 0, meaning that $\Delta\Delta G^0_{np} + \Delta\Delta G^0_{elc} + \Delta\Delta G^0_{lip} = -8.8$ kcal mol$^{-1}$.

The most recent attempt to measure $\Delta G_{whf}$ is that of Hunt et al (53, 54). They discovered that a 36-residue peptide containing the C helix of bacteriorhodopsin could be caused to insert spontaneously into lipid bilayers as a TM $\alpha$-helix by lowering pH and thereby protonating one of the two Asp residues located within the known TM domain of bR (44). The insertion followed an interfacial pathway because they found that the C-helix peptide binds to the surface of DMPC vesicles in a largely unfolded form at pH $= 7.8$ (Asp deprotonated), but inserts reversibly upon lowering the pH. From their data, they estimated a value for the free energy of insertion of about $-6$ kcal mol$^{-1}$. This value probably does not correspond to $\Delta G_{whf}$ because the peptide was neither helical nor monomeric in the aqueous phase. If the peptide had been unfolded, but monomeric, their measurement would have been of $\Delta G_{wf} + \Delta G_{whf}$, a valuable number to have. Unfortunately, the aggregation problem, as Hunt et al recognized, makes the meaning of their value for the free energy of insertion uncertain.

## THE COMPACT STATE OF MEMBRANE PROTEINS: HELIX-HELIX INTERACTIONS

The major role of the hydrophobic effect in MPs is to favor the establishment of secondary structure elements across the lipid bilayer. Given that the hydrophobic effect is generally considered the major driving force for compactness of soluble proteins, the question of why MPs are compact within a nonpolar environment merits close attention. The answer to that question must surely be important for understanding the stability of soluble proteins because, after all, the interiors of membrane and soluble proteins are very similar. The following discussion shows that van der Waals forces, more specifically the London dispersion force (25, 91), must be the dominant stabilizing force responsible for the specificity of helix-helix interactions of MPs.

### *Theoretical Considerations*

Detailed studies of model hydrophobic TM helices in phospholipid bilayers (103, 185–187) disclose four important facts. First, the structures and motions of the TM helices are little affected by lipids above, below, or at their gel-to-liquid crystal phase transitions. Helices are generally quite rigid, consistent with the great stability of H-bonds in TM helices, but the degree of rigidity depends somewhat on amino-acid (185) and lipid composition (186). Second,

the lipid phase adapts its thickness to the length of the nonpolar region of the helix, consistent with the expectations of the hydrophobic mismatch concept (reviewed in 106). Third, the behavior of the lipids of the bilayer is profoundly affected by the presence of TM helices, even at very low concentrations. Fourth, a TM helix affects ~20 lipids in its immediate neighborhood, which is about the number expected to pack around the helix periphery (103). This "boundary" lipid has modified acyl-chain conformations and is in rapid exchange with the lipids in "peptide-poor" domains (55, 144). Stated in a simplistic way, these findings show that the lipids are relatively "soft" and the TM helices are relatively "hard" and that the lipids in the immediate neighborhood of helices are perturbed.

With these ideas in mind, following the approach of Lemmon & Engelman (82), the helix-helix association term $\Delta G_{ha}$ in Figure 4 can be described by

$$\Delta G_{ha} = \Delta G_{H\text{-}H} + n\Delta G_{L\text{-}L} - 2n\Delta G_{H\text{-}L} + \Delta G_{cofact}, \qquad 4.$$

in which $\Delta G_{H\text{-}H}$, $\Delta G_{L\text{-}L}$, and $\Delta G_{H\text{-}L}$ represent the free energies for helix-helix, lipid-lipid, and helix-lipid interactions, respectively. A free energy term $\Delta G_{cofact}$ has been added to include situations in which cofactors, such as retinal in bacteriorhodopsin (see below), affect stability. This equation assumes that for $2n$ lipid molecules returned to the bilayer upon helix association, $n$ lipid-lipid interactions are gained and $2n$ helix-lipid interactions are lost.

A number of possibilities for favorable and unfavorable contributions to $\Delta G_{ha}$ arise from the various terms (82). Earlier discussion showed that favorable contributions to $\Delta G_{H\text{-}H}$ from salt-bridge, H-bonding, and other specific polar interactions between helices are unlikely to be universally important. The remaining possibilities for favorable contributions to $\Delta G_{H\text{-}H}$ interactions include helix-dipole and van der Waals–London interactions. Van der Waals–London forces may also be important in the $\Delta G_{L\text{-}L}$ and $\Delta G_{H\text{-}L}$ owing to inefficient packing of lipid acyl chains against the helix surface and relatively better packing between lipid chains. The packing inefficiency of acyl chains is likely to depend on transbilayer position because NMR measurements show that acyl chains have more disorder near the bilayer center than near the interface (see for example 137). The acyl chains may therefore be more adaptable to a TM helix near the bilayer center. Packing of the lipids against the relatively rigid helices may order the acyl chains with unfavorable entropic consequences for $\Delta G_{H\text{-}L}$. Nonspecific bilayer effects will contribute to $\Delta G_{H\text{-}L}$ and $\Delta G_{L\text{-}L}$, but presently there are few direct data relevant to their effect on $\Delta G_{ha}$, nor is there a theoretical framework for including it, except possibly through hydrophobic mismatch schemes (see 47, 104, 106).

An important broad question is whether there is any general tendency for hydrophobic TM helices to aggregate in lipid bilayers in nonspecific ways.

An often-invoked mechanism for helix association is helix-dipole interactions that are in principle very favorable for antiparallel arrangements in nonpolar phases (30, 183). A continuum electrostatic analysis (8) suggests, however, that this is unlikely. Although fully buried helices (i.e. including termini) are strongly attracted ($\Delta G_{ha} \approx -6$ kcal mol$^{-1}$), the attraction is greatly diminished ($\Delta G_{ha} \approx -1$ kcal mol$^{-1}$) when the termini extend beyond the hydrocarbon core (the usual case for TM helices) because of the partial charges on the termini. These results suggest that there are unlikely to be any substantial nonspecific interactions between helices in bilayers.

An estimate for $\Delta G_{ha}$ for biologically relevant helices can be surmised from studies of the stability of bacteriorhodopsin refolded in membranes from contiguous fragments (discussed more fully below). The tendency of contiguous helix fragments A, B, and CDEFG of bR (Figure 11) to reassemble in lipid vesicles to form a stable lattice of trimers of native-like protein depends strongly on the P:L ratio (66, 67), the optimal molar ratio being 1:30 to 1:60. This ratio is about equivalent to surrounding the seven-helix bundle with one or two layers of phospholipid (92). Based on measurements of the absorbance maximum ($\lambda_{max}$) of the retinal of bR, a major change in the bR conformation occurs at P:L = 1:300, and apparently complete dissociation of the bR fragments occurs at 1:3000. These results suggest that, despite very specific interactions that lead to native-like bR at very high protein concentrations, the interactions are not sufficiently strong to overcome the entropic advantage of dilution by lipids at very low P:L ratios. A simple model (147, 176) for aggregation provides a useful estimate of $\Delta G_{ha}$. Consider helix monomers H in equilibrium with very large aggregates of $n$ helices characterized by an association parameter $s$, so that $H_{n-1} + H \overset{s}{\leftrightarrow} H_n$. Using P:L concentration units (176), the total helix concentration $C_T$ will be related to the monomer concentration $C_m$ by (147) $C_T = C_m/(1 - sC_m)^2$. There will be a distribution of aggregate sizes of mean size (176) $\overline{n} = (1 - sC_m)^{-1}$, and the free energy of transfer of a monomer into an aggregate will be (176)

$$\Delta G_{m\to a} = -RT \ln s. \qquad 5.$$

For $\overline{n} = 100$ and a monomer concentration of 0.0003 helices per lipid (P:L = 1:3000), $\Delta G_{m\to a}$ would have to be about $-4.7$ kcal mol$^{-1}$. For P:L ratios of 1:300 and 1:30, the required values of $\Delta G_{m\to a}$ would be $-3.5$ and $-2.0$ kcal mol$^{-1}$, respectively. The latter values provide very rough estimates of $\Delta G_{ha}$ for the helices of bR.

Another estimate for $\Delta G_{ha}$ can be obtained by assuming that the association of helices is due to van der Waals–London interactions arising from poor packing of lipid chains next to a helix. The free energy cost of creating a cavity within the core of soluble proteins has been estimated experimentally as

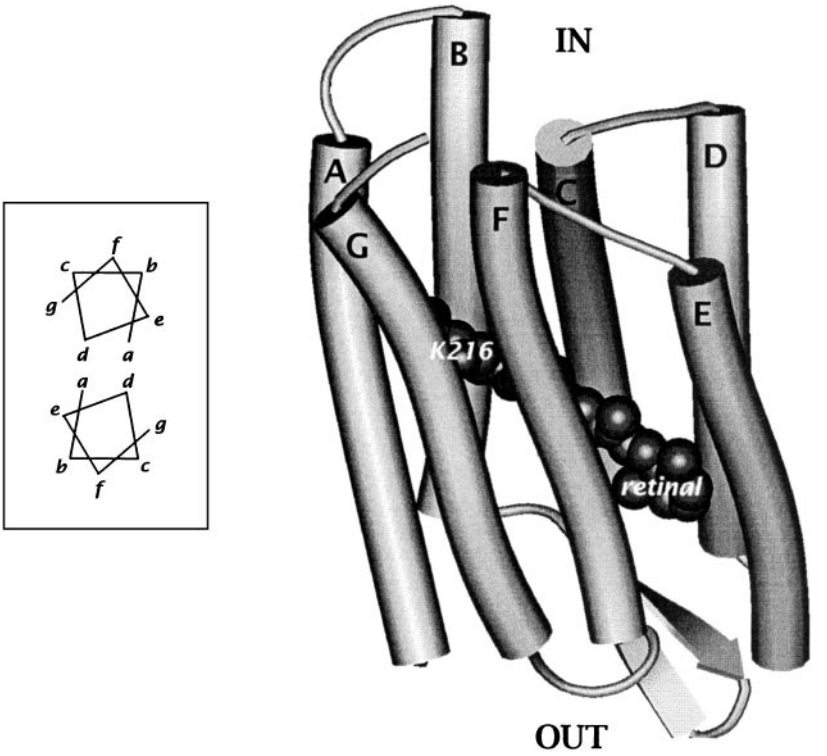


*Figure 11* Schematic representation of bacteriorhodopsin (bR). The seven TM helices of bR are shown as cylinders and the retinal linked to lysine 216 (K216) by a Schiff base is shown as a space-filling model. The figure is constructed from the crystallographic structure of Luecke et al (87) (2.3 Å resolution. PDB coordinates 1BRX). Protein reconstituted from contiguous helical bR fragments [(AB•CDEFG) and (A•B•CDEFG)] into membrane sheets has a similar structure at a resolution of 7 Å (66). A study (93) of the stability of bR reconstituted into phospholipid/detergent micelles from various complementary fragment combinations (AB•CDEFG, ABC•DEFG, ABCD•EFG, etc) shows that all seven helices must be present for proper assembly of bR, but that no single connecting link is indispensable. However, the CD and EF connecting links are more important than the others in maintaining the specificity of bR helix interactions. *Inset*: Top view of the heptad repeat motif of $\alpha$-helices in a coiled-coil configuration. The motif of the helix-bundle of bR is left-handed coiled-coils (17, 80). Examination of the meshworks of the residue-residue contacts of the helix-helix interfaces of several helix-bundle proteins disclose that meshing residues at helix-helix interfaces fit a heptad repeat pattern, with the meshing residues occurring at positions *a*, *d*, *e*, or *g*. Unlike soluble coiled-coils that prefer nonpolar residues at positions *a* and *d* and polar ones at *e* and *g*, membrane helix-bundle proteins show little preference for particular residues at interfacial positions; the preferences are about the same as the general preference of membrane-buried domains for hydrophobic residues (80).

30 cal mol$^{-1}$ Å$^{-3}$ (40). The cost of creating a void of volume 54 Å$^3$ (the volume of a methyl group) is therefore about 1.6 kcal mol$^{-1}$. If helix-helix packing relative to helix-lipid packing improved packing efficiency by an amount equivalent to the volume of 2–3 methyls, the free energy reduction favoring helix association would be 3–5 kcal mol$^{-1}$, which compares favorably with the estimates of $\Delta G_{m\rightarrow a}$ calculated using Equation 5. This suggests that the van der Waals–London force is responsible for driving MPs into a compact state, but additional contributions arising from bilayer effects cannot be eliminated. The attractive feature of van der Waals–London interactions is that their optimization inherently involves specificity, which is a requirement for assembling properly folded MPs.

## *The Compact State of Helix Bundle Proteins: Left-Handed Coiled-Coils*

A survey (17) of the packing of the TM helices of bacteriorhodopsin, photosynthetic reaction centers, and cytochrome c oxidase reveals that the 88 TM helices examined are tilted relative to the bilayer normal on average by 21° and with respect to one another by an average value of +20°. The mean distance of closest approach between helices is 9.6 Å, about the same as for soluble proteins. A recent general analysis of "knob-into-hole" packing of helices (158) indicates that the preferred packing angles of helices are −37°, +83°, and +22°. Thus, the average left-handed packing angle of +20° observed for the helix-bundle proteins suggests a knob-into-hole packing arrangement. Closer examination (80) showed this presumption to be correct—helix-bundle MPs have the general structural features of left-handed coiled-coils, characteristic of fibrous proteins and leucine zippers [coiled-coils are succinctly reviewed in (88)]. Examination of the meshworks of the residue-residue contacts of the helix-helix interfaces disclosed that nearly all (97%) of the interfacial residues fit a heptad repeat pattern (see inset, Figure 11).

## *Thermal Stability of a Helix-Bundle Protein: Bacteriorhodopsin*

Bacteriorhodopsin, perhaps the most exhaustively studied of all MPs, is an archetypal $\alpha$-helix-bundle protein (Figure 11) whose structural features conform to the general characteristics of MPs. The beauty of bR as a representative MP is that the spectroscopic properties of its retinal cofactor are exquisitely sensitive to bR's physical state, making it possible to assess bR's state in studies of stability. Differential scanning calorimetry (DSC) permits the partial heat capacities $C_p$ of proteins to be measured as a function of temperature, from which thermal transition temperatures $T_m$ and enthalpies of denaturation $\Delta H_d$ can be determined (reviewed in 116). Calorimetric and X-ray studies (50, 59)

of purple membranes from *Halobacterium salinarium*, in which bR trimers are arranged in a hexagonal crystalline lattice, disclose two thermal transitions: a reversible one at ~80°C with $\Delta H_d = 8$ kcal mol$^{-1}$ and an irreversible one at ~100°C with $\Delta H_d = 100$ kcal mol$^{-1}$. The general picture that emerges from the studies is that bR monomers reversibly change their conformation at 80° (19), causing dissociation of the lattice into a dispersion of bR trimers. At around 100°, the trimers dissociate into monomers accompanied by irreversible unfolding. The most important feature of bR melting is that the dissociation of bR trimers, which are stabilized by helix-helix interactions between monomers, involves a very significant absorption of heat arising from favorable interaction energies that do not involve the hydrophobic effect.

At least three possibilities exist for the favorable association of the bR helices: direct helix-helix interactions, helix-retinal interactions, and interactions associated with helix connecting links (CL) such as CL-interface and CL-helix interactions. Kahn et al (67) addressed these questions through calorimetric studies of intact bR helices and of contiguous helical bR fragments [(AB•CDEFG) and (A•B•CDEFG) in Figure 11] reconstituted into membrane sheets and vesicles in the presence and absence of retinal at various pHs. Their general findings were 1. The denaturation of native bR is accompanied by an enthalpy of denaturation of 100 to 179 kcal mol$^{-1}$, depending on sample preparation (vesicles or sheets) and method of measurement (DSC, optical absorbance, CD); 2. retinal has the dominant effect on bR thermal stability; removing it reduces the enthalpy of denaturation by 60 to 100 kcal mol$^{-1}$; and 3. when retinal is present, breaking the BC connecting link reduces the enthalpy of denaturation by 33 to 89 kcal mol$^{-1}$, whereas breakage of both AB and BC links (vesicles only) reduces enthalpy of denaturation by 82 to 145 kcal mol$^{-1}$. Two important conclusions follow from these results. First, the specificity of helix-helix packing does not depend on the connecting links. Rather, it must arise from the knob-into-hole packing, consistent with van der Waals interactions being important to stability. Second, the connecting links and retinal are important for overall stability, but not specificity. This focuses attention on the contribution of interfacial interactions of the connecting links to membrane stability.

A recent study (93) of the stability of bR reconstituted into phospholipid/detergent micelles from various complementary fragment combinations (AB•CDEFG, ABC•DEFG, ABCD•EFG, etc) indicates that the CD and EF connecting links are more important than the others in maintaining the specificity of bR helix interactions (Figure 11). This is interesting in the context of recent studies of the stabilities of individual bR helices in vesicles (53, 54), which show that only helices A, B, D, and E form independently stable TM helices, but as discussed earlier, helix C will form a stable TM helix upon protonation

of its aspartate residues. Helix F did not form any stable secondary structure, and helix G formed some sort of hyper-stable $\beta$-sheet structure. Combined, these results suggest that the CD and EF connecting links may be important in the formation and stability of helices C, F, and G.

## *Helix Dimers: Glycophorin A*

Although these studies of bR demonstrate the likely importance of van der Waals–driven knob-into-hole packing for the specificity and stability of helix-helix interactions, the intrinsic helix-helix interactions are difficult to separate from contributions of retinal and the helix connecting links. Extensive studies of the dimerization of the single-helix TM protein glycophorin A (GpA) have permitted the intrinsic interactions to be examined in considerable detail (reviewed in 16, 82). Lemmon & Engelman and their colleagues, in a remarkable series of papers, examined the specificity of the TM helix interactions through mutational (83, 84) and computational analyses (149), surmised the essential elements of a dimerization motif for the segment, and proposed that the helix dimer formed a right-handed coiled-coil. A subsequent study in which all TM residues outside the dimerization motif were mutated to leucines demonstrated convincingly that the dimerization motif of GpA is $L^{75}I^{76}xxG^{79}V^{80}xxG^{83}V^{84}xxT^{87}$ (85). A preliminary computational model suggested a $-30^\circ$ crossing angle, which was subsequently revised to $-45^\circ$ in a more comprehensive modeling study (1).

MacKenzie et al (90) delivered the coup de grâce by means of an NMR determination of the three-dimensional structure of the GpA dimer in SDS (90). The structure of the dimerization domain, shown in Figure 12, was extraordinarily close to the one predicted from the mutational and computational work. Several new mutational strategies have recently been developed that are providing additional information about the dimerization motif (18, 99, 100). Of particular interest is a study (18) in which an in vivo system was used for detecting dimerization, rather than the usual in vitro SDS system. Valines in positions 80 and 84 in the motif were not required for stability in natural membranes, suggesting that detergent-solubilized dimers might have a skewing effect. The crucial part of the motif in natural membranes is therefore $G^{79}xxxG^{83}$.

The next advances in the continuing saga of GpA dimerization must focus on quantitative determinations of the energetics of dimerization. Fleming et al (42) examined the energetics of GpA dimerization in detergent micelles by means of analytical ultracentrifugation, and found that the substitutions $Leu^{75} \rightarrow Ala$ and $Ile^{76} \rightarrow Ala$ destabilized the dimer by 1.1 kcal $mol^{-1}$ and 1.7 kcal $mol^{-1}$, respectively, in pentaoxyethylene octyl ether ($C_8E_5$) detergent micelles. Modeling studies that began with the known GpA dimer structure led to the conclusion that the Ala substitutions reduced the interchain buried molecular surface areas by about 80 $Å^2$. Using an experimentally determined van der Waals free

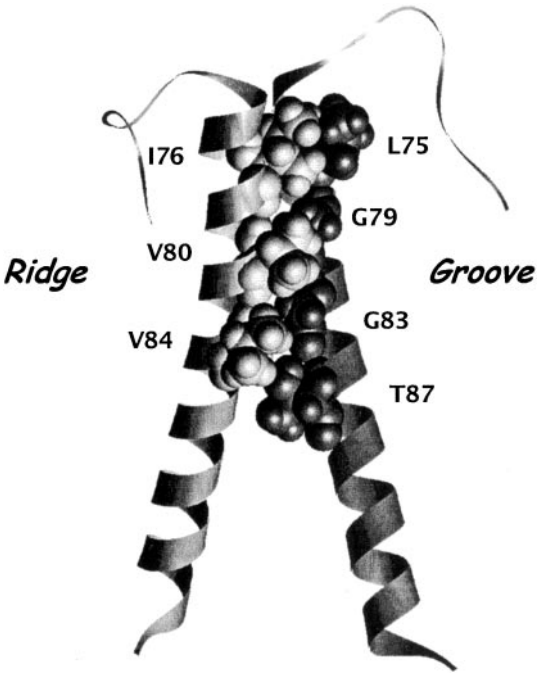


*Figure 12* The structure of the dimer of glycophorin A in detergent micelles determined using NMR methods (90). The $C_\alpha$ backbones of the helices are shown as *ribbons* and the side chains comprising the contact surfaces as *space-filling models*. The structure consists of a right-handed supercoil of helices with a $-40^\circ$ crossing angle [the theoretically expected crossing angle is $-37^\circ$ (158)] and, as anticipated, the helices mesh in a knob-into-hole or, more accurately, a ridge-into-groove arrangement. The ridge is formed by the valines and isoleucine of the motif and the groove by the glycines and threonine, completely consistent with the specificity and compactness expected from van der Waals interactions. The knob-into-hole packing can be completely disrupted by seemingly innocuous substitutions, such as Gly83 $\rightarrow$ Ala. Structure constructed from PDB coordinates 1AFO.

energy parameter of 20 cal mol$^{-1}$ Å$^{-2}$ (40), the calculated destabilizing effect of the Ala substitutions was found to be 1.6 kcal mol$^{-1}$, consistent with the experimental number.

MacKenzie & Engelman (89) have developed a structure-based algorithm for analyzing and predicting the energetics of GpA dimerization based on mutational analyses (84, 99, 100, 149), which allows coarse quantitation of the effects of the various mutants. Even though the algorithm is highly empirical and operates on a relative (and more or less arbitrary) energy scale, it nevertheless yields sharp insights into the dominant interactions controlling dimerization. The idea of the algorithm is to use the coarsely scored mutation results (four levels of stability, scored from 0 to 3) to determine the coefficients *k*, *A*, *B*, and *C*, in formulas such as

$$calc = k + A \cdot clsh + B \cdot dsrot + C \cdot vdw, \qquad 6.$$

where *calc* is the calculated relative stability and *clsh*, *dsrot*, and *vdw* represent the contributions of steric clash, side chain rotamer entropy, and van der Waals interactions, respectively. Other models that included side chain hydrophobicity and volume were shown statistically not to be effective. Most encouraging is that a plot of values of *calc* from Equation 6 against the free energies of dissociation from the centrifugation analysis (42) yielded a straight line and consequently a calibration of the empirical four-level stability scale. The calibration of Equation 6 suggests that a single step in the four-level empirical scale corresponds to a dissociation free energy of 1 kcal mol$^{-1}$. The range of free energies is about 4 kcal mol$^{-1}$, very similar to the helix-helix interaction free energies $\Delta G_{m\rightarrow a}$ estimated above (Equation 5). Thus, $\Delta G_{ha}$ in the four-step thermodynamic cycle (Figure 4) seems to be in the range of 1–5 kcal mol$^{-1}$ for helices in stably folded MPs.

## IMPLICATIONS FOR PROTEIN FOLDING

Progress in protein folding and structure prediction has evolved around several persistent themes. One of the themes is "dominant forces" in protein folding (35, 69) concerned most often with the relative contributions of hydrogen bonding and the hydrophobic effect to protein stability, and occasionally van der Waals–London forces (116) and secondary-structure desolvation energies (181). Another theme, "hierarchical folding," holds that folding proceeds by the formation of secondary structure elements, followed by collapse into the final folded state (117). "Packing determines structure" (123), a third theme, posits that a protein's final compact structure is determined uniquely by the three-dimensional jigsaw puzzle of the meshing of side chains. There are other themes, of course, but the work reviewed here brings these three to mind.

There is little doubt that the hydrophobic effect (146), which causes water to expel nonpolar solutes, is the dominant force driving initial collapse of an unfolded chain toward the folded state—a collapse that is opposed by the unfavorable cost of desolvating secondary structure (181). The image of what happens between this initial event and the final compaction is rather vague for soluble proteins. If the hierarchical folding theme has merit, a condition is presumably reached in which the elements of secondary structure come into close proximity as water extrudes itself from between the elements as the finale of the hydrophobic effect. Such a condition would be equivalent in membrane proteins to the "establishment" (113) of secondary structure elements across the membrane. Other forces would have to take control at that point in the folding process—forces that undoubtedly arise from a balance of electrostatic forces of all sorts, among them the van der Waals–London force (25, 91). The interactions of helices with one another within the hydrocarbon core of the bilayer reveal the importance of this force. The interiors of membrane and soluble proteins are virtually indistinguishable. One must therefore conclude that the final compaction process of soluble proteins, as for membrane proteins, is driven by van der Waals–London forces, as concluded by Privalov (116) through indirect arguments.

The two-stage model for protein folding of Popot & Engelman (113) is hierarchical folding in a different guise. It is a neat one. With membrane proteins, freed from the worry of exactly how, when, and why the secondary structure elements form, one can focus more clearly on the final compaction event. The experiments with bacteriorhodopsin and other membrane proteins show that, even with disrupted external connecting loops, TM helices can find their way to the final compact state. This state, the unique one encoded in the amino acid sequence, is a result of the fitting together of the "knobs" into their proper "holes," as in the fitting together of cylindrical jigsaw puzzle pieces. If it works for membrane proteins, it must surely work for soluble proteins. Perhaps the idea (125) of trying to solve the 3D jigsaw puzzle of soluble proteins should be revisited. Membrane proteins may be a good place to start.

Even with membrane proteins, one must eventually return to a consideration of the physics that shape secondary structure elements. Studies of the folding of peptides in membrane interfaces (78, 176, 179) shed light on this subject. The hydrophobic effect and Coulombic attraction drive unfolded and partially folded peptides into the bilayer interface, where they experience an environment intermediate between water and pure hydrocarbon. Even though this environment is "wet," burial of peptide bonds is energetically costly. Hydrogen bonding can reduce the cost, and secondary structure is the result. One can speculate that this interfacial environment mimics the environment of collapsing chains of soluble proteins. A closer examination of electrostatic forces in

the bilayer interfacial environment may therefore help us to understand what goes on in soluble proteins during compaction.

The interactions of the polypeptide chains of a protein with each other and with the surrounding medium determine the protein's structure and stability. The study of soluble proteins is both simplified and complicated by the bulk aqueous phase. It is simplified in that a bulk aqueous phase is easier to comprehend than the anisotropic and inhomogeneous bilayer phase. It is complicated by the fact that the aqueous phase provides few limitations on the structural motifs accessible to the polypeptide chain. For membrane proteins, although the environment is complicated, the bilayer imposes thermodynamic and geometric constraints that limit the number of accessible structural motifs. The advantage that MPs offer in the study of protein folding is that events interconnected in complex ways in soluble proteins can be disentangled to a remarkable extent.

## ACKNOWLEDGMENTS

This work was supported in part by a grant from the National Institute of General Medical Sciences (GM46823). We thank Mr. Michael Myers for his editorial assistance and Drs. Kalina Hristova, Alexey Ladokhin, and Ronald McElhaney for useful discussions.



*Literature Cited*

1. Adams PD, Engelman DM, Brünger AT. 1996. Improved prediction for the structure of the dimeric transmembrane domain of glycophorin A obtained through global searching. *Proteins* 26:257–61
2. Andrews DW, Johnson AE. 1996. The translocon: more than a hole in the ER membrane? *Trends Biochem. Sci.* 21: 365–69
3. Anfinsen CB. 1973. Principles that govern the folding of protein chains. *Science* 181:223–30
4. Arkin IT, Brünger AT, Engelman DM. 1997. Are there dominant membrane protein families with a given number of helices? *Proteins* 28:465–66
5. Bechinger B. 1996. Towards membrane protein design: pH-sensitive topology of histidine-containing polypeptides. *J. Mol. Biol.* 263:768–75
6. Ben-Shaul A, Ben-Tal N, Honig B. 1996. Statistical thermodynamic analysis of peptide and protein insertion into lipid membranes. *Biophys. J.* 71:130–37
7. Ben-Tal N, Ben-Shaul A, Nicholls A, Honig B. 1996. Free-energy determinants of $\alpha$-helix insertion into lipid bilayers. *Biophys. J.* 70:1803–12
8. Ben-Tal N, Honig B. 1996. Helix-helix interactions in lipid bilayers. *Biophys. J.* 71:3046–50
9. Ben-Tal N, Honig B, Peitzsch RM, Denisov G, McLaughlin S. 1996. Binding of small basic peptides to membranes containing acidic lipids: theoretical models and experimental results. *Biophys. J.* 71:561–75
10. Ben-Tal N, Sitkoff D, Topol IA, Yang A-S, Burt SK, Honig B. 1997. Free energy of amide hydrogen bond formation in vacuum, in water, and in liquid alkane solution. *J. Phys. Chem. B* 101:450–57
11. Bibi E. 1998. The role of the ribosome-translocon complex in translation and assembly of polytopic membrane proteins. *Trends Biochem. Sci.* 23:51–55
12. Bibi E, Kaback HR. 1990. In vivo expression of the lacY gene in two

segments leads to functional lac permease. *Proc. Natl. Acad. Sci. USA* 87:4325–29
13. Blobel G, Dobberstein B. 1975. Transfer of proteins across membranes. I. Presence of proteolytically processed and unprocessed nascent immunoglobulin light chains on membrane-bound ribosomes of murine myeloma. *J. Cell Biol.* 67:835–51
14. Blondelle SE, Forood B, Houghten RA, Pérez-Payá E. 1997. Secondary structure induction in aqueous vs. membrane-like environments. *Biopolymers* 42:489–98
15. Booth PJ, Riley ML, Flitsch SL, Templer RH, Farooq A, et al. 1997. Evidence that bilayer bending rigidity affects membrane protein folding. *Biochemistry* 36:197–203
16. Bormann BJ, Engelman DM. 1992. Intramembrane helix-helix association in oligomerization and transmembrane signaling. *Annu. Rev. Biophys. Biomol. Struct.* 21:223–42
17. Bowie JU. 1997. Helix packing in membrane proteins. *J. Mol. Biol.* 272:780–89
18. Brosig B, Langosch D. 1998. The dimerization motif of the glycophorin A transmembrane segment in membranes: importance of glycine residues. *Protein Sci.* 7:1052–56
19. Brouillette CG, McMichens RB, Stern LJ, Khorana HG. 1989. Structure and thermal stability of monomeric bacteriorhodopsin in mixed phospholipid/detergent micelles. *Proteins* 5:38–46
19a. Buchanan SK, Smith BS, Venkatramani L, Xia D, Esser L, et al. 1999. Crystal structure of the outer membrane active transporter FepA from *Escherichia coli*. *Nat. Struct. Biol.* 6:56–63
20. Chan HS, Dill KA. 1997. Solvation: how to obtain microscopic energies from partitioning and solvation experiments. *Annu. Rev. Biophys. Biomol. Struct.* 26: 425–59
21. Chang CH, Elkabbani O, Tiede D, Norris J, Schiffer M. 1991. Structure of the membrane-bound protein photosynthetic reaction center from *Rhodobacter sphaeroides*. *Biochemistry* 30:5352–60
21a. Chang G, Spencer RH, Lee AT, Barclay MT, Rees DC. 1998. Structure of the MscL homolog from *Mycobacterium tuberculosis*: a gated mechanosensitive ion channel. *Science* 282:2220–26
22. Charifson PS, Hiskey RG, Pedersen LG. 1997. Construction and molecular modeling of phospholipid surfaces. *J. Comput. Chem.* 11:1181–86
23. Chothia C. 1974. Hydrophobic bonding and accessible surface area in proteins. *Nature* 248:338–39
24. Chothia C. 1975. Structural invariants in protein folding. *Nature* 254:304–8
25. Chu B. 1967. *Molecular Forces* (based on the Baker lectures of Peter JW Debye). New York: Wiley. 176 pp.
26. Cowan SW, Schirmer T, Rummel G, Steiert M, Ghosh R, et al. 1992. Crystal structures explain functional properties of two *E. coli* porins. *Nature* 358:727–33
27. Cramer WA, Engelman DM, von Heijne G, Rees DC. 1992. Forces involved in the assembly and stabilization of membrane proteins. *FASEB J.* 6:3397–402
28. Cramer WA, Heymann JB, Schendel SL, Deriy BN, Cohen FS, et al. 1995. Structure-function of the channel-forming colicins. *Annu. Rev. Biophys. Biomol. Struct.* 24:611–41
29. Dathe M, Schümann M, Wieprecht T, Winkler A, Beyermann M, et al. 1996. Peptide helicity and membrane surface charge modulate the balance of electrostatic and hydrophobic interactions with lipid bilayers and biological membranes. *Biochemistry* 35:12612–22
30. Deber CM, Li S-C. 1995. Peptides in membranes: helicity and hydrophobicity. *Biopolymers* 37:295–318
31. Deisenhofer J, Epp O, Miki K, Huber R, Michel H. 1985. Structure of the protein subunits in the photosynthetic reaction centre of *Rhodospeudomonas viridis* at 3 Å resolution. *Nature* 318:618–24
32. Dempsey CE. 1990. The actions of melittin on membranes. *Biochim. Biophys. Acta* 1031:143–61
33. de Planque MRR, Greathouse DV, Koeppe RE II, Schäfer H, Marsh D, Killian JA. 1998. Influence of lipid/peptide hydrophobic mismatch on the thickness of diacylphosphatidylcholine bilayers. A 2H NMR and ESR study using designed transmembrane $\alpha$-helical peptides and gramicidin A. *Biochemistry* 37:9333–45
34. De Young LR, Dill KA. 1990. Partitioning of nonpolar solutes into bilayers and amorphous n-alkanes. *J. Phys. Chem.* 94:801–9
35. Dill KA. 1990. Dominant forces in protein folding. *Biochemistry* 29:7133–55
36. Doyle DA, Cabral JM, Pfuetzner RA, Kuo AL, Gulbis JM, et al. 1998. The structure of the potassium channel: molecular basis of $K^+$ conduction and selectivity. *Science* 280:69–77
37. Eisenberg D, Schwarz E, Komaromy M, Wall R. 1984. Analysis of membrane

and surface protein sequences with the hydrophobic moment plot. *J. Mol. Biol.* 179:125–42
38. Engelman DM, Steitz TA. 1981. The spontaneous insertion of proteins into and across membranes: the helical hairpin hypothesis. *Cell* 23:411–22
39. Engelman DM, Steitz TA, Goldman A. 1986. Identifying nonpolar transbilayer helices in amino acid sequences of membrane proteins. *Annu. Rev. Biophys. Biophys. Chem.* 15:321–53
40. Eriksson AE, Baase WA, Zhang XJ, Heinz DW, Blaber M, et al. 1992. Response of a protein structure to cavity-creating mutations and its relation to the hydrophobic effect. *Science* 255:178–83
41. Fauchère J-L, Pliska V. 1983. Hydrophobic parameters $\pi$ of amino-acid side chains from the partitioning of N-acetyl–amino-acid amides. *Eur. J. Med. Chem. C* 18:369–75
42. Fleming KG, Ackerman AL, Engelman DM. 1997. The effect of point mutations on the free energy of transmembrane $\alpha$-helix dimerization. *J. Mol. Biol.* 272:266–75
42a. Ferguson AD, Hofmann E, Coulton JW, Diederichs K, Welte W. 1998. Siderophore-mediated iron transport: crystal structure of FhuA with bound lipopolysaccharide. *Science* 282:2215–20
43. Gill SJ, Dec SF, Olofsson G, Wadsö I. 1985. Anomalous heat capacity of hydrophobic solvation. *J. Phys. Chem.* 89: 3758–61
44. Grigorieff N, Ceska TA, Downing KH, Baldwin JM, Henderson R. 1996. Electron-crystallographic refinement of the structure of bacteriorhodopsin. *J. Mol. Biol.* 259:393–421
45. Groves JD, Tanner MJA. 1995. Coexpressed complementary fragments of the human red cell ion exchanger (Band3, AE1) generate stilbene disulfonate-sensitive anion transport. *J. Biol. Chem.* 270:9097–105
46. Haltia T, Freire E. 1995. Forces and factors that contribute to the structural stability of membrane proteins. *Biochim. Biophys. Acta* 1241:295–322
47. He K, Ludtke SJ, Heller WT, Huang HW. 1996. Mechanism of alamethicin insertion into lipid bilayers. *Biophys. J.* 71:2669–79
48. Henderson R, Baldwin JM, Ceska TA, Zemlin F, Beckmann E, Downing KH. 1990. Model for the structure of bacteriorhodopsin based on high-resolution electron cryo-microscopy. *J. Mol. Biol.* 213:899–929
49. Hendsch ZS, Tidor B. 1994. Do salt bridges stabilize proteins? A continuum electrostatic analysis. *Protein Sci.* 3:211–26
50. Hiraki K, Hamanaka T, Mitsui T, Kito Y. 1981. Phase transitions of the purple membrane and the brown holomembrane: X-ray diffraction, circular dichroism spectrum and absorption spectrum studies. *Biochim. Biophys. Acta* 647:18–28
51. Hristova K, Selsted ME, White SH. 1997. Critical role of lipid composition in membrane permeabilization by rabbit neutrophil defensins. *J. Biol. Chem.* 272:24224–33
52. Hristova K, White SH. 1998. Determination of the hydrocarbon core structure of fluid dioleoylphosphocholine (DOPC) bilayers by x-ray diffraction using specific bromination of the double-bonds: effect of hydration. *Biophys. J.* 74:2419–33
53. Hunt JF, Earnest TN, Bousché O, Kalghatgi K, Reilly K, et al. 1997. A biophysical study of integral membrane protein folding. *Biochemistry* 36: 15156–76
54. Hunt JF, Rath P, Rothschild KJ, Engelman DM. 1997. Spontaneous, pH-dependent membrane insertion of a transbilayer $\alpha$-helix. *Biochemistry* 36: 15177–92
55. Huschilt JC, Hodges RS, Davis JH. 1985. Phase equilibria in an amphiphilic peptide-phospholipid model membrane by deuterium magnetic resonance difference spectroscopy. *Biochemistry* 24:1377–86
56. Hyde CC, Ahmed SA, Padlan EA, Miles EW, Davies DR. 1988. Three-dimensional structure of the tryptophan synthase $\alpha 2\beta 2$ multienzyme complex from *Salmonella typhimurium*. *J. Biol. Chem.* 263:17857–71
57. Iwata S, Lee JW, Okada K, Lee JK, Iwata M, et al. 1998. Complete structure of the 11-subunit bovine mitochondrial cytochrome bc1 complex. *Science* 281:64–71
58. Iwata S, Ostermeier C, Ludwig B, Michel H. 1995. Structure at 2.8 Å resolution of cytochrome c oxidase from *Paracoccus denitrificans*. *Nature* 376:660–69
59. Jackson MB, Sturtevant JM. 1978. Phase transitions of the purple membranes of *Halobacterium halobium*. *Biochemistry* 17:911–15

60. Jacobs RE, White SH. 1984. Behavior of hexane dissolved in dioleoylphosphatidylcholine bilayers: an NMR and calorimetric study. *J. Am. Chem. Soc.* 106:6909–12
61. Jacobs RE, White SH. 1989. The nature of the hydrophobic binding of small peptides at the bilayer interface: implications for the insertion of transbilayer helices. *Biochemistry* 28:3421–37
62. Jähnig F. 1983. Thermodynamics and kinetics of protein incorporation into membranes. *Proc. Natl. Acad. Sci. USA* 80:3691–95
63. Janin J. 1996. For Guldberg and Waage, with love and cratic entropy. *Proteins* 24:i–ii
64. Johnson AE, Liao S, Lin J, Hamman B, Do H, et al. 1995. The environment of nascent secretory and membrane proteins at the endoplasmic reticulum membrane during translocation and integration. *Cold Spring Harbor Symp. Quant. Biol.* 60:71–82
65. Kaback HR, Voss J, Wu J. 1997. Helix packing in polytopic membrane proteins: the lactose permease of *Escherichia coli*. *Curr. Opin. Struct. Biol.* 7:537–42
66. Kahn TW, Engelman DM. 1992. Bacteriorhodopsin can be refolded from two independently stable transmembrane helices and the complementary five-helix fragment. *Biochemistry* 31:6144–51
67. Kahn TW, Sturtevant JM, Engelman DM. 1992. Thermodynamic measurements of the contributions of helix-connecting loops and of retinal to the stability of bacteriorhodopsin. *Biochemistry* 31:8829–39
68. Kaiser ET, Kézdy FJ. 1983. Secondary structures of proteins and peptides in amphiphilic environments (a review). *Proc. Natl. Acad. Sci. USA* 80:1137–43
69. Kauzmann W. 1959. Some factors in the interpretation of protein denaturation. *Adv. Protein Chem.* 14:1–63
70. Khan SMA, Bolen W, Hargrave PA, Santoro MM, McDowell JH. 1991. Differential scanning calorimetry of bovine rhodopsin in rod-outer-segment disk membranes. *Eur. J. Biochem.* 200:53–59
71. Kimura Y, Vassylyev DG, Miyazawa A, Kidera A, Matsushima M, et al. 1997. Surface of bacteriorhodopsin revealed by high-resolution electron crystallography. *Nature* 389:206–11
72. Kleinschmidt JH, Tamm LK. 1996. Folding intermediates of a $\beta$-barrel membrane protein. Kinetic evidence for a multi-step membrane insertion mechanism. *Biochemistry* 35:12993–3000
73. Koebnik R. 1996. In vivo membrane assembly of split variants of the *E. coli* outer membrane protein OmpA. *EMBO J.* 15:3529–37
74. Koepke J, Hu XC, Muenke C, Schulten K, Michel H. 1996. The crystal structure of the light-harvesting complex II (B800–850) from *Rhodospirillum molischianum*. *Structure* 4:581–97
75. Kurumbail RG, Stevens AM, Gierse JK, McDonald JJ, Stegeman RA, et al. 1996. Structural basis for selective inhibition of cyclooxygenase-2 by anti-inflammatory agents. *Nature* 384:644–48
76. Kühlbrandt W, Wang DN, Fujiyoshi Y. 1994. Atomic model of plant light-harvesting complex by electron crystallography. *Nature* 367:614–21
77. Kyte J, Doolittle RF. 1982. A simple method for displaying the hydropathic character of a protein. *J. Mol. Biol.* 157: 105–32
78. Ladokhin AS, White SH. 1999. Folding of amphipathic $\alpha$-helices on membranes: energetics of helix formation by melittin. *J. Mol. Biol.* 285:1363–69
79. Landolt-Marticorena C, Williams KA, Deber CM, Reithmeier RAF. 1993. Non-random distribution of amino acids in the transmembrane segments of human type I single span membrane proteins. *J. Mol. Biol.* 229:602–8
80. Langosch D, Heringa J. 1998. Interaction of transmembrane helices by a knobs-into-holes packing characteristic of soluble coiled coils. *Proteins* 31:150–59
81. Lau FW, Bowie JU. 1997. A method for assessing the stability of a membrane protein. *Biochemistry* 36:5884–92
82. Lemmon MA, Engelman DM. 1994. Specificity and promiscuity in membrane helix interactions. *Q. Rev. Biophys.* 27:157–218
83. Lemmon MA, Flanagan JM, Hunt JF, Adair BD, Bormann BJ, et al. 1992. Glycophorin-A dimerization is driven by specific interactions between transmembrane $\alpha$-helices. *J. Biol. Chem.* 267: 7683–89
84. Lemmon MA, Flanagan JM, Treutlein HR, Zhang J, Engelman DM. 1992. Sequence specificity in the dimerization of transmembrane alpha-helices. *Biochemistry* 31:12719–25
85. Lemmon MA, Treutlein HR, Adams PD, Brünger AT, Engelman DM. 1994. A dimerization motif for transmembrane

alpha-helices. *Nat. Struct. Biol.* 1:157–63
86. Li S-C, Deber CM. 1994. A measure of helical propensity for amino acids in membrane environments. *Nat. Struct. Biol.* 1:368–73
87. Luecke H, Richter HT, Lanyi JK. 1998. Proton transfer pathways in bacteriorhodopsin at 2.3 Angstrom resolution. *Science* 280:1934–37
88. Lupas A. 1996. Coiled coils: new structures and new functions. *Trends Biochem. Sci.* 21:375–82
89. MacKenzie KR, Engelman DM. 1998. Structure-based prediction of the stability of transmembrane helix-helix interactions: the sequence dependence of glycophorin A dimerization. *Proc. Natl. Acad. Sci. USA* 95:3583–90
90. MacKenzie KR, Prestegard JH, Engelman DM. 1997. A transmembrane helix dimer: structure and implications. *Science* 276:131–33
91. Mahanty J, Ninham BW. 1976. *Dispersion Forces*. London: Academic. 236 pp.
92. Marsh D. 1997. Stoichiometry of lipid-protein interaction and integral membrane protein structure. *Eur. Biophys. J.* 26:203–8
93. Marti T. 1998. Refolding of bacteriorhodopsin from expressed polypeptide fragments. *J. Biol. Chem.* 273:9312–22
94. Matlack KES, Mothes W, Rapoport TA. 1998. Protein translocation: tunnel vision. *Cell* 92:381–90
95. McDermott G, Prince SM, Freer AA, Hawthornthwaite-Lawless AM, Papiz MZ, et al. 1995. Crystal structure of an integral membrane light-harvesting complex from photosynthetic bacteria. *Nature* 374:517–21
96. McDonnell PA, Shon K, Kim Y, Opella SJ. 1993. fd coat protein structure in membrane environments. *J. Mol. Biol.* 233:447–63
97. Meyer JEW, Hofnung M, Schulz GE. 1997. Structure of maltoporin from *Salmonella typhimurium* ligated with a nitrophenyl-maltotrioside. *J. Mol. Biol.* 266:761–75
98. Milik M, Skolnick J. 1993. Insertion of peptide chains into lipid membranes: an off-lattice Monte Carlo dynamics model. *Proteins* 15:10–25
99. Mingarro I, Elofsson A, von Heijne G. 1997. Helix-helix packing in a membrane-like environment. *J. Mol. Biol.* 272:633–41
100. Mingarro I, Whitley P, Lemmon MA, von Heijne G. 1996. Ala-insertion scanning mutagenesis of the glycophorin A transmembrane helix: a rapid way to map helix-helix interactions in integral membrane proteins. *Protein Sci.* 5:1339–41
101. Moll TS, Thompson TE. 1994. Semisynthetic proteins: model systems for the study of the insertion of hydrophobic peptides into preformed lipid bilayers. *Biochemistry* 33:15469–82
102. Morein S, Strandberg E, Killian JA, Persson S, Arvidson G, et al. 1997. Influence of membrane-spanning $\alpha$-helical peptides on the phase behavior of the dioleoylphosphatidylcholine/water system. *Biophys. J.* 73:3078–88
103. Morrow MR, Huschilt JC, Davis JH. 1985. Simultaneous modeling of phase and calorimetric behavior in an amphiphilic peptide/phospholipid model membrane. *Biochemistry* 24:5396–406
104. Mouritsen OG, Biltonen RL. 1993. Protein-lipid interactions and membrane heterogeneity. In *Protein-Lipid Interactions*, ed. A Watts, pp. 1–39. Amsterdam: Elsevier
105. Mouritsen OG, Bloom M. 1984. Mattress model of lipid-protein interactions in membranes. *Biophys. J.* 46:141–53
106. Mouritsen OG, Bloom M. 1993. Models of lipid-protein interactions in membranes. *Annu. Rev. Biophys. Biomol. Struct.* 22:145–71
107. Oren Z, Shai Y. 1997. Selective lysis of bacteria but not mammalian cells by diastereomers of melittin: structure-function study. *Biochemistry* 36:1826–35
108. Pace CN. 1986. Determination and analysis of urea and guanidine hydrochloride denaturation curves. *Methods Enzymol.* 131:266–80
108a. Pautsch A, Schulz GE. 1998. Structure of the outer membrane protein A transmembrane domain. *Nat. Struct. Biol.* 5:1013–17
109. Pebay-Peyroula E, Rummel G, Rosenbusch JP, Landau EM. 1997. X-ray structure of bacteriorhodopsin at 2.5 Å from microcrystals grown in lipidic cubic phases. *Science* 277:1676–81
110. Persson S, Killian JA, Lindblom G. 1998. Molecular ordering of interfacially localized tryptophan analogs in ester- and ether-lipid bilayers studied by 2H-NMR. *Biophys. J.* 75:1365–71
111. Picot D, Loll PJ, Garavito RM. 1994. The X-ray crystal structure of the membrane protein prostaglandin H2 synthase-1. *Nature* 367:243–49
112. Pitzer KS. 1995. *Thermodynamics*. New York: McGraw-Hill. 626 pp. 3rd ed.

113. Popot J-L, Engelman DM. 1990. Membrane protein folding and oligomerization—the 2-stage model. *Biochemistry* 29:4031–37
114. Popot J-L, Gerchman S-E, Engelman DM. 1987. Refolding of bacteriorhodopsin in lipid bilayers. A thermodynamically controlled two-stage process. *J. Mol. Biol.* 198:655–76
115. Preusch PC, Norvell JC, Cassatt JC, Cassman M. 1998. Progress away from 'no crystals, no grant'. *Nat. Struct. Biol.* 5:12–14
116. Privalov PL. 1992. Physical basis of the stability of the folded conformations of proteins. In *Protein Folding*, ed. TE Creighton, pp. 83–126. New York: Freeman
117. Ptitsyn OB. 1992. The molten globule state. See Ref. 116, pp. 243–300
118. Rees DC, Chirino AJ, Kim K-H, Komiya H. 1994. Membrane protein structure and stability: implications of the first crystallographic analyses. See Ref. 163, pp. 3–26
119. Rees DC, De Antonio L, Eisenberg D. 1989. Hydrophobic organization of membrane proteins. *Science* 245:510–13
120. Rees DC, Komiya H, Yeates TO, Allen JP, Feher G. 1989. The bacterial photosynthetic reaction center as a model for membrane proteins. *Annu. Rev. Biochem.* 58:607–33
121. Reithmeier RAF. 1995. Characterization and modeling of membrane proteins using sequence analysis. *Curr. Opin. Struct. Biol.* 5:491–500
122. Reynolds JA, Gilbert DB, Tanford C. 1974. Empirical correlation between hydrophobic free energy and aqueous cavity surface area. *Proc. Natl. Acad. Sci. USA* 71:2925–27
123. Richards FM. 1977. Areas, volumes, packing, and protein structure. *Annu. Rev. Biophys. Bioeng.* 6:151–76
124. Richards FM. 1992. Folded and unfolded proteins: an introduction. See Ref. 116, pp. 1–58
125. Richards FM, Lim WA. 1993. An analysis of packing in the protein folding problem. *Q. Rev. Biophys.* 26:423–98
126. Richardson JS. 1981. The anatomy and taxonomy of protein structure. *Adv. Protein Chem.* 34:167–339
127. Ridge KD, Lee SSJ, Yao LL. 1995. In vivo assembly of rhodopsin from expressed polypeptide fragments. *Proc. Natl. Acad. Sci. USA* 92:3204–8
128. Rose GD. 1978. Prediction of chain turns in globular proteins on a hyrophobic basis. *Nature* 272:586–90
129. Rose GD, Geselowitz AR, Lesser GJ, Lee RH, Zehfus MH. 1985. Hydrophobicity of amino acid residues in globular proteins. *Science* 229:834–38
130. Roseman MA. 1988. Hydrophobicity of the peptide C=O · · · H–N hydrogen-bonded group. *J. Mol. Biol.* 201:621–25
131. Russell CJ, Thorgeirsson TE, Shin Y-K. 1996. Temperature dependence of polypeptide partitioning between water and phospholipid bilayers. *Biochemistry* 35:9526–32
132. Samatey FA, Xu C, Popot J-L. 1995. On the distribution of amino acid residues in transmembrane $\alpha$-helix bundles. *Proc. Natl. Acad. Sci. USA* 92:4577–81
133. Schatz G, Dobberstein B. 1996. Common principles of protein translocation across membranes. *Science* 271:1519–26
134. Schiffer M, Chang CH, Stevens FJ. 1992. The functions of tryptophan residues in membrane proteins. *Protein Eng.* 5:213–14
135. Schubert W-D, Klukas O, Krauss N, Saenger W, Fromme P, Witt HT. 1997. Photosystem I of *Synechococcus elongatus* at 4 Å resolution: comprehensive structure analysis. *J. Mol. Biol.* 272:741–69
136. Schwarz G. 1996. Electrical interactions of membrane active peptides at lipid/water interfaces. *Biophys. Chem.* 58:67–73
137. Seelig A, Seelig J. 1974. The dynamic structure of fatty acyl chains in a phospholipid bilayer measured by deuterium magnetic resonance. *Biochemistry* 13:4839–45
138. Seelig J, Ganz P. 1991. Nonclassical hydrophobic effect in membrane binding equilibria. *Biochemistry* 30:9354–59
139. Sharp KA, Nicholls A, Friedman R, Honig B. 1991. Extracting hydrophobic free energies from experimental data: relationship to protein folding and theoretical models. *Biochemistry* 30:9686–97
140. Simon SA, Stone WL, Busto-Latorre P. 1977. A thermodynamic study of the partition of n-hexane into phosphatidylcholine and phosphatidylcholine-cholesterol bilayers. *Biochim. Biophys. Acta* 468:378–88
141. Simon SM. 1995. Protein-conducting channels for the translocation of proteins into and across membranes. *Cold Spring Harbor Symp. Quant. Biol.* 60:57–69
142. Soekarjo M, Eisenhawer M, Kuhn A,

Vogel H. 1996. Thermodynamics of the membrane insertion process of the M13 procoat protein, a lipid bilayer traversing protein containing a leader sequence. *Biochemistry* 35:1232–41
143. Song L, Hobaugh MR, Shustak C, Cheley S, Bayley H, Gouaux JE. 1996. Structure of staphylococcal $\alpha$-hemolysin, a heptameric transmembrane pore. *Science* 274:1859–66
144. Subczynski WK, Lewis RNAH, McElhaney RN, Hodges RS, Hyde JS, Kusumi A. 1998. Molecular organization and dynamics of 1-palmitoyl-2-oleoylphosphatidylcholine bilayers containing a transmembrane $\alpha$-helical peptide. *Biochemistry* 37:3156–64
145. Surrey T, Schmid A, Jähnig F. 1996. Folding and membrane insertion of the trimeric $\beta$-barrel protein OmpF. *Biochemistry* 35:2283–88
146. Tanford C. 1973. *The Hydrophobic Effect: Formation of Micelles and Biological Membranes*. New York: Wiley 200 pp. 1st ed.
147. Terzi E, Hölzemann G, Seelig J. 1994. Reversible random coil-$\dot{\beta}$-sheet transition of the Alzheimer $\beta$-amyloid fragment. *Biochemistry* 33:1345–50
148. Thorgeirsson TE, Yu YG, Shin Y-K. 1995. A limiting law for the electrostatics of the binding of polypeptides to phospholipid bilayers. *Biochemistry* 34:5518–22
149. Treutlein HR, Lemmon MA, Engelman DM, Brünger AT. 1992. The glycophorin A transmembrane domain dimer: sequence-specific propensity for a right-handed supercoil of helices. *Biochemistry* 31:12726–33
150. Tristram-Nagle S, Yang C-P, Nagle JF. 1986. Thermodynamic studies of purple membrane. *Biochim. Biophys. Acta* 854:58–66
151. Tsukihara T, Aoyama H, Yamashita E, Tomizaki T, Yamaguchi H, et al. 1996. The whole structure of the 13-subunit oxidized cytochrome c oxidase at 2.8 Å. *Science* 272:1136–44
152. Vogel H. 1981. Incorporation of melittin into phosphatidylcholine bilayers: study of binding and conformational changes. *FEBS Lett.* 134:37–42
153. von Heijne G. 1992. Membrane protein structure prediction—hydrophobicity analysis and the positive-inside rule. *J. Mol. Biol.* 225:487–94
154. von Heijne G. 1994. Membrane proteins: from sequence to structure. *Annu. Rev. Biophys. Biomol. Struct.* 23:167–92
155. Waldburger CD, Schildbach JF, Sauer RT. 1995. Are buried salt bridges important for protein stability and conformational specificity? *Nat. Struct. Biol.* 2:122–28
156. Wallin E, Tsukihara T, Yoshikawa S, von Heijne G, Elofsson A. 1997. Architecture of helix bundle membrane proteins: an analysis of cytochrome c oxidase from bovine mitochondria. *Protein Sci.* 6:808–15
157. Wallin E, von Heijne G. 1998. Genome-wide analysis of integral membrane proteins from eubacterial, archaean, and eukaryotic organisms. *Protein Sci.* 7: 1029–38
158. Walther D, Eisenhaber F, Argos P. 1996. Principles of helix-helix packing in proteins: the helical lattice superposition model. *J. Mol. Biol.* 255:536–53
159. Weiss MS, Abele U, Weckesser J, Welte W, Schiltz E, Schulz GE. 1991. Molecular architecture and electrostatic properties of a bacterial porin. *Science* 254:1627–30
160. Weiss MS, Schulz GE. 1992. Structure of porin refined at 1.8 Å resolution. *J. Mol. Biol.* 227:493–509
161. White SH. 1977. Studies of the physical chemistry of planar bilayer membranes using high precision measurements of specific capacitance. *Ann. NY Acad. Sci.* 303:243–65
162. White SH. 1980. How electric fields modify alkane solubility in lipid bilayers. *Science* 207:1075–77
163. White SH. 1994. Hydropathy plots and the prediction of membrane protein topology. In *Membrane Protein Structure: Experimental Approaches*, ed. SH White, pp. 97–124. New York: Oxford Univ. Press
164. White SH, King GI, Cain JE. 1981. Location of hexane in lipid bilayers determined by neutron diffraction. *Nature* 290:161–63
165. White SH, Wiener MC. 1995. Determination of the structure of fluid lipid bilayer membranes. In *Permeability and Stability of Lipid Bilayers*, ed. EA Disalvo, SA Simon, pp. 1–19. Boca Raton, FL: CRC Press
166. White SH, Wiener MC. 1996. The liquid-crystallographic structure of fluid lipid bilayer membranes. In *Membrane Structure and Dynamics*, ed. KM Merz, B Roux, pp. 127–44. Boston: Birkhäuser
167. White SH, Wimley WC. 1994. Peptides in lipid bilayers: structural and thermodynamic basis for partitioning and folding. *Curr. Opin. Struct. Biol.* 4:79–86

168. White SH, Wimley WC. 1998. Hydrophobic interactions of peptides with membrane interfaces. *Biochim. Biophys. Acta* 1376:339–52
169. White SH, Wimley WC, Ladokhin AS, Hristova K. 1998. Protein folding in membranes: determining the energetics of peptide-bilayer interactions. *Methods Enzymol.* 295:62–87
170. Wiener MC, White SH. 1991. Fluid bilayer structure determination by the combined use of X-ray and neutron diffraction. I. Fluid bilayer models and the limits of resolution. *Biophys. J.* 59: 162–73
171. Wiener MC, White SH. 1991. Fluid bilayer structure determination by the combined use of X-ray and neutron diffraction. II. "Composition-space" refinement method. *Biophys. J.* 59:174–85
172. Wiener MC, White SH. 1992. Structure of a fluid dioleoylphosphatidylcholine bilayer determined by joint refinement of X-ray and neutron diffraction data. III. Complete structure. *Biophys. J.* 61:434–47
173. Wieprecht T, Dathe M, Epand RM, Beyermann M, Krause E, et al. 1997. Influence of the angle subtended by the positively charged helix face on the membrane activity of amphipathic, antibacterial peptides. *Biochemistry* 36: 12869–80
174. Wimley WC, Creamer TP, White SH. 1996. Solvation energies of amino acid sidechains and backbone in a family of host-guest pentapeptides. *Biochemistry* 35:5109–24
175. Wimley WC, Gawrisch K, Creamer TP, White SH. 1996. A direct measurement of salt-bridge solvation energies using a peptide model system: implications for protein stability. *Proc. Natl. Acad. Sci. USA* 93:2985–90
176. Wimley WC, Hristova K, Ladokhin AS, Silvestro L, Axelsen PH, White SH. 1998. Folding of $\beta$-sheet membrane proteins: a hydrophobic hexapeptide model. *J. Mol. Biol.* 277:1091–110
177. Wimley WC, White SH. 1992. Partitioning of tryptophan side-chain analogs between water and cyclohexane. *Biochemistry* 31:12813–18
178. Wimley WC, White SH. 1993. Membrane partitioning: distinguishing bilayer effects from the hydrophobic effect. *Biochemistry* 32:6307–12
179. Wimley WC, White SH. 1996. Experimentally determined hydrophobicity scale for proteins at membrane interfaces. *Nat. Struct. Biol.* 3:842–48
180. Xia D, Yu C-A, Kim H, Xia J-Z, Kachurin AM, et al. 1997. Crystal structure of the cytochrome bc1 complex from bovine heart mitochondria. *Science* 277:60–66
181. Yang A-S, Sharp KA, Honig B. 1992. Analysis of the heat capacity dependence of protein folding. *J. Mol. Biol.* 227:889–900
182. Yau W-M, Wimley WC, Gawrisch K, White SH. 1998. The preference of tryptophan for membrane interfaces. *Biochemistry* 37:14713–18
183. Yeates TO, Komiya H, Rees DC, Allen JP, Feher G. 1987. Structure of the reaction center from *Rhodobacter sphaeroides* R-26: membrane-protein interactions. *Proc. Natl. Acad. Sci. USA* 84:6438–42
184. Zhan H, Oh KJ, Shin Y–K, Hubbell WL, Collier RJ. 1995. Interaction of the isolated transmembrane domain of diphtheria toxin with membranes. *Biochemistry* 34:4856–63
185. Zhang Y-P, Lewis RNAH, Henry GD, Sykes BD, Hodges RS, McElhaney RN. 1995. Peptide models of helical hydrophobic transmembrane segments of membrane proteins. 1. Studies of the conformation, intrabilayer orientation, and amide hydrogen exchangeability of Ac-K2-(LA)12-K2-amide. *Biochemistry* 34:2348–61
186. Zhang Y-P, Lewis RNAH, Hodges RS, McElhaney RN. 1995. Peptide models of helical hydrophobic transmembrane segments of membrane proteins. 2. Differential scanning calorimetric and FTIR spectroscopic studies of the interaction of Ac-K2-(LA)12-K2-amide with phosphatidylcholine bilayers. *Biochemistry* 34:2362–71
187. Zhang YP, Lewis RNAH, Hodges RS, McElhaney RN. 1992. Interaction of a peptide model of a hydrophobic transmembrane alpha-helical segment of a membrane protein with phosphatidylcholine bilayers—differential scanning calorimetric and FTIR spectroscopic studies. *Biochemistry* 31:11579–88
188. Zhang ZL, Huang LS, Shulmeister VM, Chi Y-I, Kim KK, et al. 1998. Electron transfer by domain movement in cytochrome bc1. *Nature* 392:677–84